

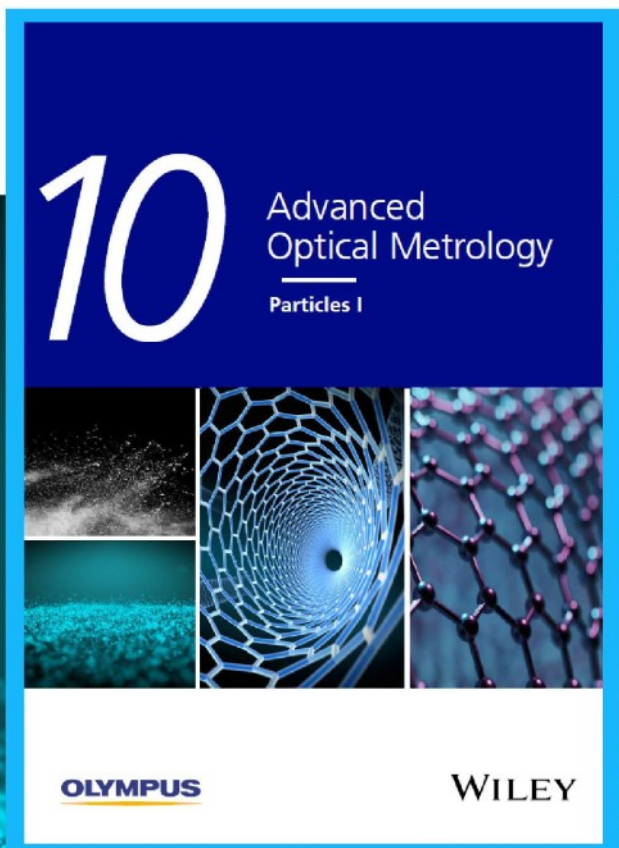


Particles I

Access the latest eBook →

Particles: Unique Properties,
Uncountable Applications

**Read the latest eBook and
better your knowledge with
highlights from the recent
studies on the design and
characterization of micro-
and nanoparticles for
different application areas.**



Access Now

This eBook is sponsored by

OLYMPUS

WILEY

Lithium-Diffusion Induced Capacity Losses in Lithium-Based Batteries

David Rehnlund,* Zhaohui Wang, and Leif Nyholm

Rechargeable lithium-based batteries generally exhibit gradual capacity losses resulting in decreasing energy and power densities. For negative electrode materials, the capacity losses are largely attributed to the formation of a solid electrolyte interphase layer and volume expansion effects. For positive electrode materials, the capacity losses are, instead, mainly ascribed to structural changes and metal ion dissolution. This review focuses on another, so far largely unrecognized, type of capacity loss stemming from diffusion of lithium atoms or ions as a result of concentration gradients present in the electrode. An incomplete delithiation step is then seen for a negative electrode material while an incomplete lithiation step is obtained for a positive electrode material. Evidence for diffusion-controlled capacity losses is presented based on published experimental data and results obtained in recent studies focusing on this trapping effect. The implications of the diffusion-controlled Li-trapping induced capacity losses, which are discussed using a straightforward diffusion-based model, are compared with those of other phenomena expected to give capacity losses. Approaches that can be used to identify and circumvent the diffusion-controlled Li-trapping problem (e.g., regeneration of cycled batteries) are discussed, in addition to remaining challenges and proposed future research directions within this important research area.

1. Introduction

Owing to their high energy densities, Li-ion batteries (LIBs) currently dominate the mobile power source market and

significant work is carried out to improve their long-term cycling stabilities.^[1,2] However, like most electrochemical energy storage devices, LIBs generally exhibit capacity decays during repetitive charge and discharge.^[3,4] The capacity losses seen for positive electrodes are mainly ascribed to structural changes involving, for example, gas release at high potentials and transition-metal dissolution.^[5-7] For negative electrodes undergoing alloying and/or conversion reactions, the capacity losses are generally attributed to the formation of a solid electrolyte interphase (SEI) and gradual inactivation of the active material due to the large volume changes taking place during the cycling.^[8-10] A range of approaches have been developed to address the capacity decay, including the use of conductive coatings enhancing the electronic conductivity of electrodes,^[11-13] reduced active particle sizes to shorten the diffusion lengths and to reduce the mechanical strain within the electrodes,^[14-16] as well as modifications of the composition of the


electrolyte to stabilize the SEI layer.^[17-19] Nevertheless, capacity losses can still be observed for optimized electrodes composed of nanoparticles with efficient ionic/electronic networks and SEI-stabilizing electrolytes.^[3,20-26] It is, therefore, reasonable to assume that there is, at least one, additional phenomenon affecting the cycling stability of lithium-based batteries.

When reviewing the literature, it becomes evident that there are many experimental results suggesting that trapped (or irreversibly immobilized) lithium capacity can yield capacity losses. Many of these results were obtained as a result of the use of new electrode characterization procedures facilitating the detection of trapped lithium and lithium concentration gradients in cycled electrodes. Incomplete delithiation has, for example, been identified in studies involving comparisons of pristine and delithiated cycled electrodes composed of, for example, Si,^[20,21,27-30] Sn,^[28,31] Al,^[32-35] TiO₂,^[36] LiFePO₄ (LFP),^[37-39] LiNi_{1/3}Co_{1/3}Mn_{1/3}O₂(NCM),^[40] V₂O₅,^[41-44] MoO₃,^[45] LiCoO₂ (LCO),^[46] as well as ordered^[47,48] and disordered carbon.^[49-54] A large amount of diffusion-controlled trapped elemental lithium (i.e., 3.3 mol Li per mol Si) was, for example, found in optimized nano-silicon composite electrodes after 650 cycles of capacity limited (i.e., 1200 mAh g⁻¹) cycling.^[20] Lithium-ion-trapping has also been reported to give rise to a loss of performance for electrochromic thin films based on WO₃ and NiO,^[55,56] undergoing lithiation and delithiation in analogy with lithium-ion battery

D. Rehnlund, L. Nyholm
Department of Chemistry – Ångström
Uppsala University
Box 538, Uppsala SE-75121, Sweden
E-mail: david.rehnlund@kemi.uu.se

D. Rehnlund
Institute for Applied Materials – Energy Storage Systems (IAM-ESS)
Karlsruhe Institute of Technology (KIT)
Hermann-von-Helmholtz Platz 1, Eggenstein-Leopoldshafen 76344,
Germany

Z. Wang
College of Materials Science and Engineering
Hunan University
Changsha 410082, China

 The ORCID identification number(s) for the author(s) of this article can be found under <https://doi.org/10.1002/adma.202108827>.

© 2022 The Authors. Advanced Materials published by Wiley-VCH GmbH. This is an open access article under the terms of the Creative Commons Attribution License, which permits use, distribution and reproduction in any medium, provided the original work is properly cited.

DOI: 10.1002/adma.202108827

materials. Elemental lithium has likewise been found to be able to diffuse into metallic current collectors.^[28,57,58] Very long cycling times would, however, most likely be needed for this diffusion-controlled effect to become significant when a conventionally thick layer of a lithium alloy-forming active material is present on the current collector. Unlike other capacity decay mechanisms, for example, SEI formation and volume expansion effects, the diffusion-controlled Li-trapping phenomenon is still relatively unknown, despite the fact that incomplete delithiations of electrode materials have been reported by many researchers. In the latter cases, the effect was commonly ascribed to sluggish lithium diffusion and/or the formation of irreversible phases.^[10,38] In more recent work, the diffusion-controlled trapping phenomenon has been explained based on a two-way diffusion process,^[20,28] since the lithium atoms or ions in the electrode may diffuse both toward the electrode surface and toward the current collector (i.e., further into the electrode) during the delithiation step.

The aim of this review is to evaluate the experimental evidence for the diffusion-controlled Li-trapping effect based on published experimental data and proposed trapping models. The influence of Li-trapping is also compared with that of other phenomena known to give rise to capacity losses. In this review, Li-trapping will be used as a general term for the immobilization of Li in an electrode material either in the form of Li atoms (in alloy-forming materials) or Li ions (in intercalation-based electrode materials). The focus is on the evaluation of experimental data indicating the presence of a diffusion-controlled Li-trapping effect, as well as discussions of trends, challenges, and directions of future research aimed at identifying and preventing such lithium trapping. Because diffusion-controlled Li-trapping can give rise to significant capacity losses it is important to study the influence of this trapping effect on different electrode materials. As will be described in more detail below, such studies are best performed with half-cells comprising Li-metal electrodes. Since diffusion-controlled Li-trapping should be seen for alloy-forming materials as well as for intercalation-based materials it is reasonable to assume that an improved understanding of this effect can pave the way for lithium-based batteries with significantly improved long-term cycling performances, or even approaches enabling the regeneration of nonfunctioning rechargeable batteries.

2. Which Phenomena Can Give Rise to The Capacity Losses?

The performance of Li-based batteries can be affected by many reversible and irreversible capacity loss mechanisms. In this section, we will review the most widely recognized mechanisms and discuss how well these mechanisms can explain the capacity losses typically seen during the cycling of Li-based batteries.

2.1. SEI Formation and Volume Expansion Effects

For negative electrodes, the most recognized capacity loss mechanism involves the formation of the SEI layer via irreversible

reduction of the electrolyte.^[24,59] This reaction, which proceeds until the electrode surface becomes passivated,^[9,59] typically takes place in parallel with the reduction (i.e., lithiation) of the negative electrode. Capacity losses due to SEI formation are, however, mainly a problem for full-cell batteries as the SEI process then drains the capacity of the positive electrode (which typically is capacity limiting). A continuous capacity decay seen during the cycling of a full-cell can therefore be explained by an unstable SEI layer, for example, due to volume expansion effects or SEI components dissolving in the electrolyte.^[28,60] In the latter case, the SEI layer needs to be continuously reformed which results in additional draining of the positive electrode's capacity. The SEI formation can consequently be regarded as an irreversible capacity decay mechanism.^[61] Advances in electrolyte design have, however, decreased the influence of this capacity loss by enabling the formation of more stable SEI layers via the optimization of the salts, solvents, and additives used in the electrolytes.^[23,62–64] SEI forming additives such as vinylene carbonate and fluoroethylene carbonate (FEC) which are reduced at a higher potentials than the solvents (e.g., ethylene carbonate and diethylene carbonate), are often used to stabilize the SEI layers.^[23,62–64]

In a half-cell containing a high capacity Li-metal electrode, the SEI formation should, on the other hand, not give rise to any capacity losses as long as the capacity of the negative electrode remains capacity limiting.^[20,28] The SEI formation should in this case merely constitute an additional (irreversible) reduction process proceeding independently of the reduction (i.e., lithiation) of the negative electrode. While the SEI formation clearly would give rise to a decreased Coulombic efficiency, the negative electrode should still be able to undergo a complete reduction (i.e., lithiation) due to the much larger capacity of the Li-metal electrode. This can be illustrated based on the results obtained by Delpuech et al.^[65] who compared the capacity limited cycling behaviors of Si/LiCoO₂ full-cells and Si/Li half-cells (Figure 1a,b). While a constant capacity was obtained for the half-cell, a rapid capacity decay was seen for the capacity balanced full-cell. SEI formation can consequently not explain the decrease in the capacity seen for a negative electrode material cycled in a half-cell containing a Li-metal electrode. SEI formation can likewise not explain the presence of an increasing amount of trapped Li in the electrode materials, or capacity losses that can be recovered by introducing constant voltage delithiation pulses into a constant current procedure. It should also be mentioned that the capacities associated with SEI formation typically are too small to explain the capacity losses seen for most negative electrode materials.^[20,28]

Since SEI formation is generally believed to be responsible for the capacity losses seen for many electrode materials, much work has been undertaken to introduce artificial SEI layers on electrode materials. Ai et al.^[66] recently investigated the possibility of improving the cycling stability of Si electrode by using Si nanoparticles coated with a 2 nm layer of LiAlO₂. As seen in Figure 1c,d, a significantly improved cycling stability as well as a marked decrease in the amount of trapped Li was seen after 100 cycles (compare the scanning electron microscopy [SEM] images in Figure 2e–h). Although the authors ascribed the improved cycling stability (Figure 1d) to an SEI effect (which appears very unlikely since the experiments were conducted

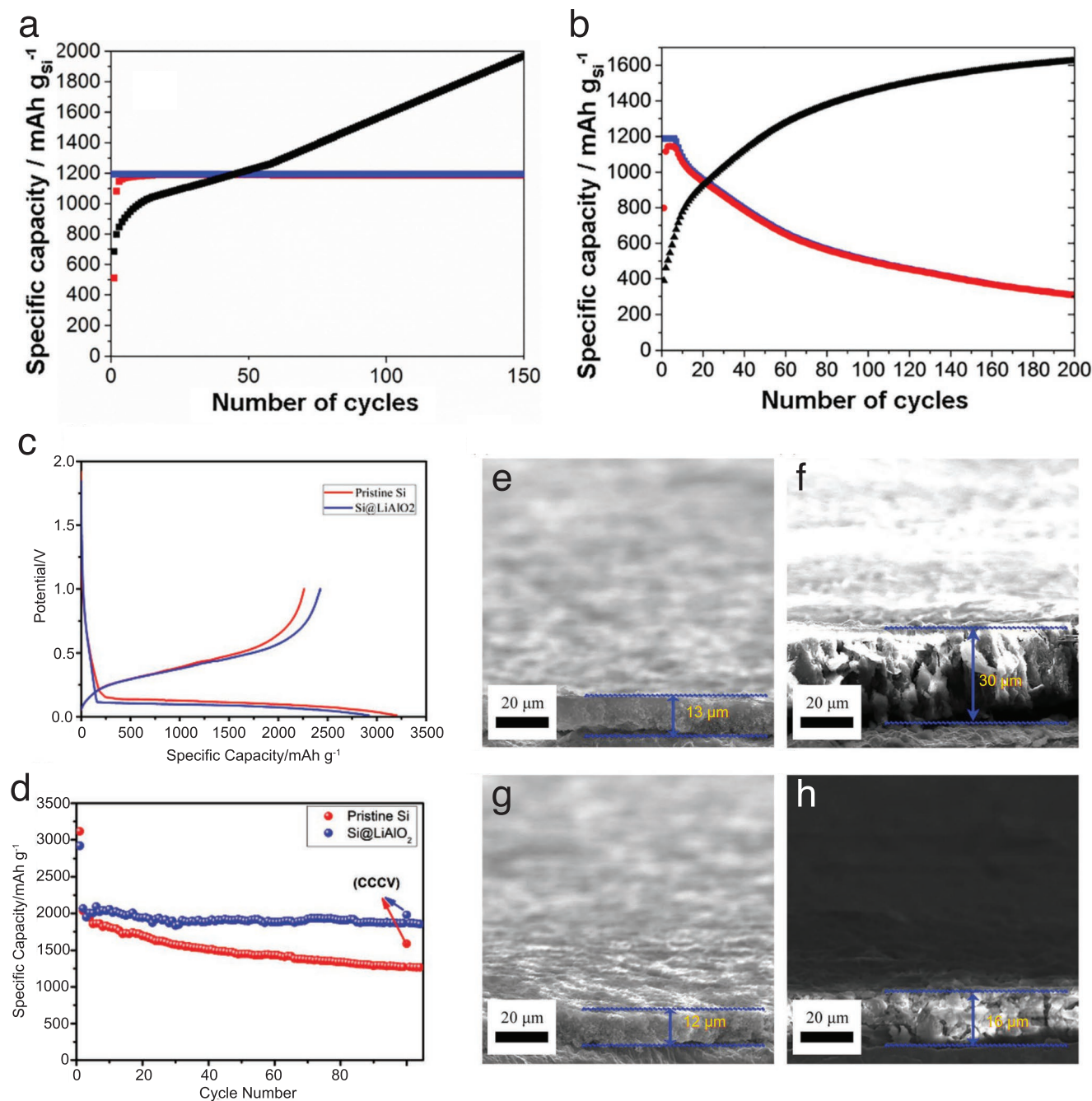


Figure 1. Specific capacity versus cycle number plots for Si electrodes cycled in a) a half-cell versus Li metal and b) a full-cell versus LiCoO₂. The specific lithiation, that is, discharge (blue) and delithiation, that is, charge (red) capacities are shown together with the corresponding cumulative irreversible capacities (black). Adapted with permission.^[65] Copyright 2016, Wiley-VCH. c–h) LiAlO₂-coated Si nanoparticles used to mitigate Li-trapping in Si electrodes. c) First cycle capacity versus voltage curves for pristine and coated Si-based electrodes and d) the corresponding specific capacities versus cycle number. e, f) SEM images of pristine Si and g, h) LiAlO₂-coated Si obtained e, g) prior to and f, h) after 100 cycles at 1000 mA g⁻¹. Adapted with permission.^[66] Copyright 2019, Wiley-VCH.

with Li-metal half-cells), the results rather indicate that the presence of the LiAlO₂ coating decreased the degree of lithiation of the Si, and hence the amount of Li trapped on each cycle. When evaluating capacity losses due to SEI formation it is consequently very important to acknowledge the differences between results obtained with full-cell batteries and those obtained with half-cells containing a high-capacity counter

electrode (e.g., a Li-metal electrode). It is likewise important to distinguish between mechanisms (such as Li-trapping and electrode degradation due to volume expansion effects) affecting the capacity of the electrode material, and reactions (such as the SEI formation) which do not directly affect the capacity of the studied electrode material.^[20] It is often suggested that an increase in the cell resistance as a result of, for example, SEI

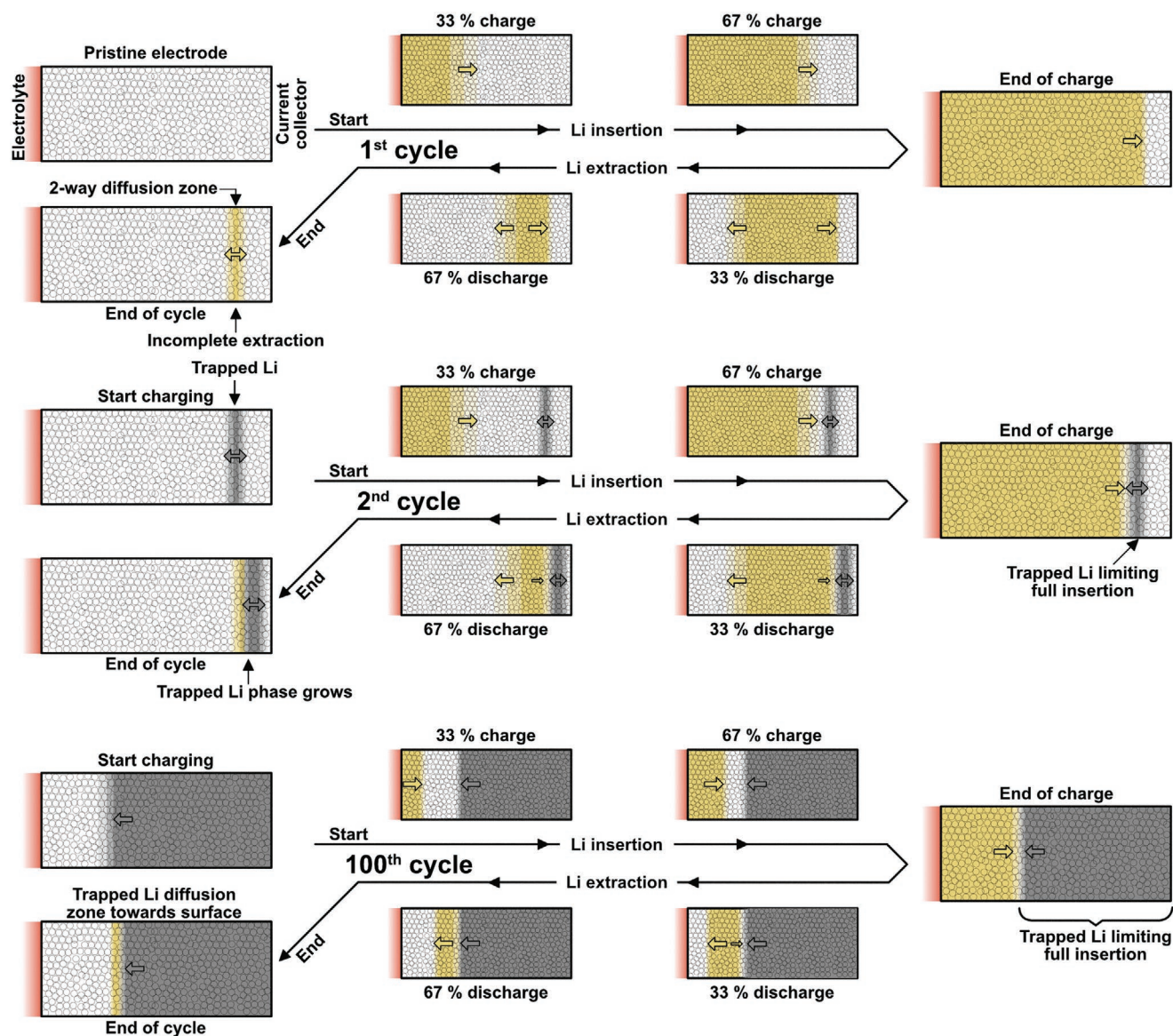


Figure 2. Schematic illustration of the diffusion-controlled Li-trapping mechanism in a composite negative electrode showing the onset during the first cycle and its effect on the second cycle as well as the progressive accumulation of the Li-trapping after extensive cycling (e.g., 100 cycles).

formation could cause the cut-off voltage limits to be reached prematurely and therefore give rise to an apparent capacity loss. Under constant current conditions, such an iR drop effect should, however, affect both the reduction and oxidation steps. It was recently shown^[20] that the increase in the Si lithiation overpotential could be explained by the increased Li concentration in the Si electrode (due to diffusion-controlled Li-trapping) and that this effect could be mitigated by using intermittent constant voltage delithiation pulses decreasing the surface concentration of Li in the Si electrode.

Although a continuous SEI formation cannot explain the decreasing capacity of an electrode material cycled in a Li-metal half-cell, it would, nevertheless, increase the apparent lithiation capacity and hence contribute to the cumulative irreversible capacity (Figure 1a,b). Analyses of the latter are very useful when trying to find the origin of capacity losses.^[28] The cumulative

irreversible capacity increases when the lithiation capacity is larger than the delithiation capacity, that is, when the Coulombic efficiency is lower than 100%, whereas a decrease indicates a delithiation capacity larger than the lithiation capacity. In the presence of an irreversible reaction (such as SEI formation), Coulombic efficiencies lower than 100% are thus expected for half-cells even when the lithiation and delithiation capacities of the electrode material are identical. This means that it is often difficult to predict the cycling stability of a half-cell using the Coulombic efficiencies.^[28,67] A half-cell exhibiting a Coulombic efficiency of 98% may hence be cycled for 300 cycles even though the remaining capacity by then would be expected to be 0.2% for a full-cell battery (as $0.98^{300} \approx 0.002$). One way of estimating the inherent reversibility of an electrode material can then be to determine an average Coulombic efficiency based on the capacity decrease seen during a specific number of cycles.^[20,28]

Another (irreversible) capacity loss mechanism often discussed, particularly in conjunction with Li-alloy forming electrode materials (e.g., Si, Sn, and Al), are the changes in the volume of the electrode material associated with the lithiation and delithiation reactions. The latter generate stress in the material which can give rise to cracking, a loss of active material and an increased electrode resistance.^[68,69] Volume expansion effects can likewise give rise to additional SEI formation as a result of an increased electrode surface area and partial loss of the SEI layer. For Si, the volume expansion upon full insertion can be as high as 280% (assuming the formation of $\text{Li}_{3.75}\text{Si}$).^[70] While it is well-known that significant losses of active material can be seen for micrometer-sized particles,^[14] the influence of the volume expansion effect can, however, be significantly decreased by using nanometer-sized alloying materials and efficient binders.^[15,31,71–75] The presence of cracking and losses of the electrode material should clearly be seen when plotting the capacity as a function of the cycle number even when using Li-metal half-cells. The volume expansion effects would, however, be expected to be particularly pronounced during the initial part of the cycling experiment. The volume expansion effect would also be expected to give rise to an irregular capacity decay rather than a continuous capacity decrease and should also be more pronounced for electrode materials undergoing large volume changes (e.g., for Si compared to Al). It is also difficult to understand why the Li concentration in the electrode material would increase during the cycling as a result of volume expansion effects, why a constant voltage delithiation step would recover of some of the lost capacity, and why the use of an extended delithiation step would extend the lifetime of an electrode. Guo and Jia recently modeled the stress evolution during Li insertion in alloy-based negative electrode materials.^[76] The study showed that stress induced during early stages of lithiation was relieved at the end of lithiation as the Li concentration profiles were homogenized over the entire particle. This indicates that rest periods between charging and discharging should relieve buildup stress inside large-volume expansion electrode materials. Rest periods should hence improve the cycling stability of these materials. As Lindgren et al. showed,^[20] this was, however, not the case for Si negative electrodes. It can therefore be concluded that while rest periods should be beneficial for decreasing the volume expansion effects, they should also increase the influence of the diffusion-controlled Li-trapping phenomenon. It is important to note that conventional cathode materials show little volume variations during electrochemical reactions and negligible SEI problems,^[77] but still suffer from capacity decay upon cycling, which indicate a capacity decay mechanism beyond volume changes and the SEI theory.

2.2. Structural Changes, Metal Ion Dissolution, and Electrolyte Oxidation

Positive electrodes typically exhibit stable cycling performances when cycled in half-cells. However, depending on the material type, initial or continuous capacity losses are generally observed. Four main mechanisms have been used to describe these capacity losses: irreversible structural changes; transition metal ion and/or oxygen dissolution; irreversible oxidation of

the electrolyte leading to the formation of the cathode electrolyte interphase (CEI) and slow Li-ion solid-state diffusion.^[5,78]

Repeated Li-intercalation and de-intercalation during cycling can often lead to structural changes causing transition metals to occupy Li^+ sites, yielding decreased Li^+ diffusion rates. Structural distortions and strain can also lead to transition metal dissolution as is commonly known for LiMn_2O_4 positive electrodes. Acidic species in the electrolyte (e.g., HF) can react with the positive electrode and preferentially leach transition metals causing their dissolution and hence a loss of capacity. Both phenomena can be effectively mitigated by the use of dopants yielding structural stabilization as well as protective coatings.^[78] Structurally driven fatigue can also lead to limited state-of-charge (SOC) cycling conditions, as was recently observed in Ni-based $\text{LiNi}_{0.8}\text{Mn}_{0.1}\text{Co}_{0.1}\text{O}_2$ (NMC) positive electrode materials.^[79,80] Surface localized reconstruction introduced a lattice mismatch between the surface and bulk material which reduced the Li diffusion rate through the material leading to $\approx 25\%$ Li remaining inside the bulk material after charge (i.e., delithiation). This repetitive process caused the population of fatigued NMC particles to increase during cycling, as each particle affected will be effectively limited to 75% SOC cycling, thereby leading to capacity decay. This structural fatigue process was described as a general feature for Ni-rich positive electrode materials (i.e., above 80% Ni content). The build-up of fatigued particles with residual Li trapped inside the bulk structure is indeed similar to diffusion-controlled Li-trapping in negative electrode materials. However, it is important to note that diffusion-controlled Li-trapping in positive electrode materials should result in a gradual decrease in the Li content of the electrode.

Many positive electrodes operate at potentials exceeding the stability window of conventional electrolytes.^[5,78] Ni-based mixed transition metal oxides (e.g., $\text{LiNi}_{1/3}\text{Mn}_{1/3}\text{Co}_{1/3}\text{O}_2$) are a prime example, in which Ni^{4+} can oxidize the electrolyte. This reaction leads to the formation of a CEI layer that passivates the electrode surface hindering further degradation of the electrolyte.^[78] Stability issues with the CEI layer due to structural strain or dissolution can lead to a continuous reformation and capacity losses. Improved cycling stability of these materials have been observed by modifying the Ni content.^[78]

Intercalation-based positive electrodes are classified by the phase transformation that takes place during Li-ion insertion/extraction.^[81,82] Materials such as LFP are classified as two-phase transformation positive electrodes, where fully delithiated regions (FePO_4) form and progressively grow leading to boundaries between delithiated (FePO_4) and lithiated (LFP) regions inside a single particle. Alternatively, materials such as LiCoO_2 undergo solid-solution transformation leading a gradual change in Li-ion concentration and no phase boundaries in the particle. This classification is important with respect to the Li-trapping mechanism as the two types lead to different Li-ion concentrations profiles inside a single particle. Recent in situ electron microscopy battery studies have,^[81,82] however, challenged this classification by showing that nanoparticles do not necessarily behave in such an ordered manner. Localized high Li-ion concentration regions in LFP were found to undergo solid-solution Li-ion movement at the nanometer scale. Controversially, creation and separation of Li-ion rich

domains was observed in LiCoO_2 thin films during lithiation where Li^+ lateral movement (i.e., toward the current collector) was observed during cycling. Cross-domain Li-ion movement was however detected when rest periods were used between the lithiation and delithiation.^[82] These results indicate that both types of positive electrode materials can exhibit unidirectional Li-ion movement at the nanometer scale. This raises the question if diffusion-controlled Li-trapping also can explain capacity losses seen for positive electrodes. Many studies have in fact indicated a strong correlation between slow Li-ion mass transfer and capacity losses. Slow Li-ion diffusion during the end stages of lithiation has been linked to first cycle capacity losses for layered metal oxide positive electrodes.^[46,79,80,83–85] This is in agreement with the observed behavior for negative electrode materials such as Si.^[20,86]

It was recently shown that Ni-based cathodes that are typically low-stress materials can crack during high SOC cycling leading to a capacity decay as intraparticle fragments become ionically disconnected from the electrolyte.^[87] This feature was, however, isolated to all solid-state batteries where the electrolyte could not penetrate the cracked cathode material. Loss of active material in solid-state batteries is therefore not necessarily an indication of diffusion-controlled Li trapping.

It is important to note that only irreversible structural changes, dissolution of active material, and slow Li-ion mass transfer can yield capacity decays for half-cells as they affect the intrinsic energy storage properties of the positive electrodes. CEI formation is, just like SEI formation, compensated by the capacity superior negative electrode (e.g., Li metal).

2.3. Diffusion-Controlled Lithium-Trapping

Energy storage devices such as Li-based batteries are based on redox reactions. When reducing an electrode material (e.g., when reducing Fe^{3+} to Fe^{2+} in LFP), a counter ion (e.g., Li^+) needs to be inserted to restore the electroneutrality of the electrode material. Energy storage is, however, also possible by directly reducing Li^+ to Li (i.e., $\text{Li}^+ + \text{e}^- = \text{Li}$) which then either is deposited on the electrode surface or forms an alloy with the negative electrode material. To simplify the discussion below, “Li” will from here on be used to describe the general process for a negative electrode involving either Li atoms or Li ions. Care should be taken when translating this mechanism to individual materials as Li atoms are incorporated in alloying electrode materials and current collectors, whereas Li ions are incorporated in intercalation-based electrode materials. For reversibility reasons, the electrode material must therefore enable balanced Li exchange during the cycling to maintain the charge storage capacity. This is, however, rarely the case as Li diffuses only into the electrode during the lithiation process whereas Li can diffuse both toward the electrode/electrolyte interface and further into the electrode core (i.e., toward the current collector) during the delithiation step. This two-way diffusion, which is schematically illustrated in Figure 2, is the origin of the diffusion-controlled Li-trapping effect since a small fraction of the Li in the electrode (or more correctly a small fraction of the lithiation charge) then becomes inaccessible on the time domain of the delithiation step.

Li is thus inserted at the electrolyte/electrode interface of the pristine electrode material causing a one-way diffusion gradient into the electrode core (i.e., toward the current collector). This process continues until the inward Li diffusion rate becomes too low to maintain the imposed current density, which causes the pre-set cut-off potential to be reached. When the electrode is delithiated, the Li extraction starts at the electrode surface (i.e., at the electrode/electrolyte interface) thereby generating the two-way diffusion seen in Figure 2. Li can now either diffuse toward the electrode surface or toward the current collector. As Li is being extracted at the electrode surface, a small portion of Li diffuses further into the electrode where it becomes increasingly more time consuming to extract. If the time domains of the Li insertion and extraction steps are the same, the diffusion-controlled Li-trapping effect will hence make it impossible to fully extract the inserted charge. During the second and subsequent cycles, the presence of the trapped Li causes the lithiation capacity to decrease as the inward diffusion rate decreases when the surface concentration of Li increases. As a result, the electrode potential is shifted negatively which causes the cut-off potential to be reached earlier. The effect of diffusion-controlled Li-trapping is thus twofold as 1) a part of the stored energy is trapped in the electrode material as well as 2) the trapped Li decreases the amount of energy that can be subsequently stored. During extended cycling the accumulated effect of repeated Li-trapping causes the electrode material to become filled with Li and the electrode reaches its (apparent) end of life. Diffusion-controlled Li-trapping is here described assuming a scenario in which $\approx 90\%$ lithiation is achieved during the first cycle, as can be the case for alloy forming anode materials such as Si. Here it should be noted that partial initial lithiation approaches, involving, for example, Coulombic limited cycling protocols, only will delay the capacity decay in half-cells and that all types of Li-trapping would cause immediate capacity decays in full-cells comprising charge balanced electrodes.^[20] Capacity limited cycling may incidentally also be (unintentionally) obtained when altering the composition of the electrolyte as the conductivity of the electrolyte affects the iR drop and hence the cycling potential window.

As the diffusion-controlled Li-trapping effect is caused by the presence of Li concentration gradients in the electrode, this trapping effect should, however, not be seen if the material can be homogeneously lithiated. While this can be realized for, for example, TiO_2 nanotube electrodes,^[36] a homogeneous lithiation is unlikely to be reached for conventional electrode materials due to the longer Li diffusion path lengths (when increasing this length from 1 nm to 1 μm , the diffusion time would be increased by a factor of one million).

While the scenario described above focuses on negative electrode materials, the diffusion-controlled Li-trapping in positive electrode materials depends on if the pristine electrode material contains lithium or not. Electrode materials that need to be prelithiated before cycling (e.g., V_2O_5 and MoO_3) should behave similarly as negative electrode materials. Positive electrodes already containing lithium (e.g., LiCoO_2 , LFP and $\text{LiNi}_x\text{Mn}_{(1-x)}\text{Co}_{(1-x)}\text{O}_2$) should, on the other hand, experience capacity losses due to diffusion-controlled Li-trapping if the delithiation during the first cycle is incomplete. As the delithiation process starts at the electrode surface and proceeds inwards toward the bulk of the electrode, a

Li concentration gradient will form. If the flux of Li toward the electrode/interface is sufficient to support the employed current, a stable redox potential can be maintained. However, an insufficient flux of Li to the electrode/interface, due to too slow Li diffusion, would induce a mass transfer limited impedance causing the redox potential to ultimately reach the cut-off potential. If the delithiation is incomplete there will hence be a lithium concentration gradient resulting in lithium diffusing toward the electrolyte/electrode interface. This opposing concentration gradient can then negatively affect the inward diffusion during subsequent lithiation causing capacity losses. In this case the lithiation degree of the positive electrode should consequently gradually decrease during the cycling, as the residual Li in the electrode prevents a full relithiation of the material to be reached.

The term “active Li loss” is often used to describe capacity losses in positive electrode materials. While it may seem like

a synonym to the term “Li-trapping,” the loss of active Li can also be due to an irreversible process if the electrode material becomes ionically or electrically disconnected from the electrolyte or current collector, respectively. In this scenario, the “active Li loss” is, however, not caused by the diffusion-controlled Li-trapping discussed in this review. Here it should be noted that while the diffusion-controlled process is inherently reversible, the accumulated capacity losses and build-up of residual Li normally are often caused by extended cycling. Repeated dedicated delithiation steps can then be employed to decrease the diffusion-controlled capacity losses and to improve the cycling stability as is shown in Figure 3b.

Essentially, there are hence two distinct kinds of Li-trapping phenomena affecting Li-based battery materials: irreversible and reversible Li-trapping. Irreversible Li-trapping can occur when Li-rich phases are ionically or electrically disconnected

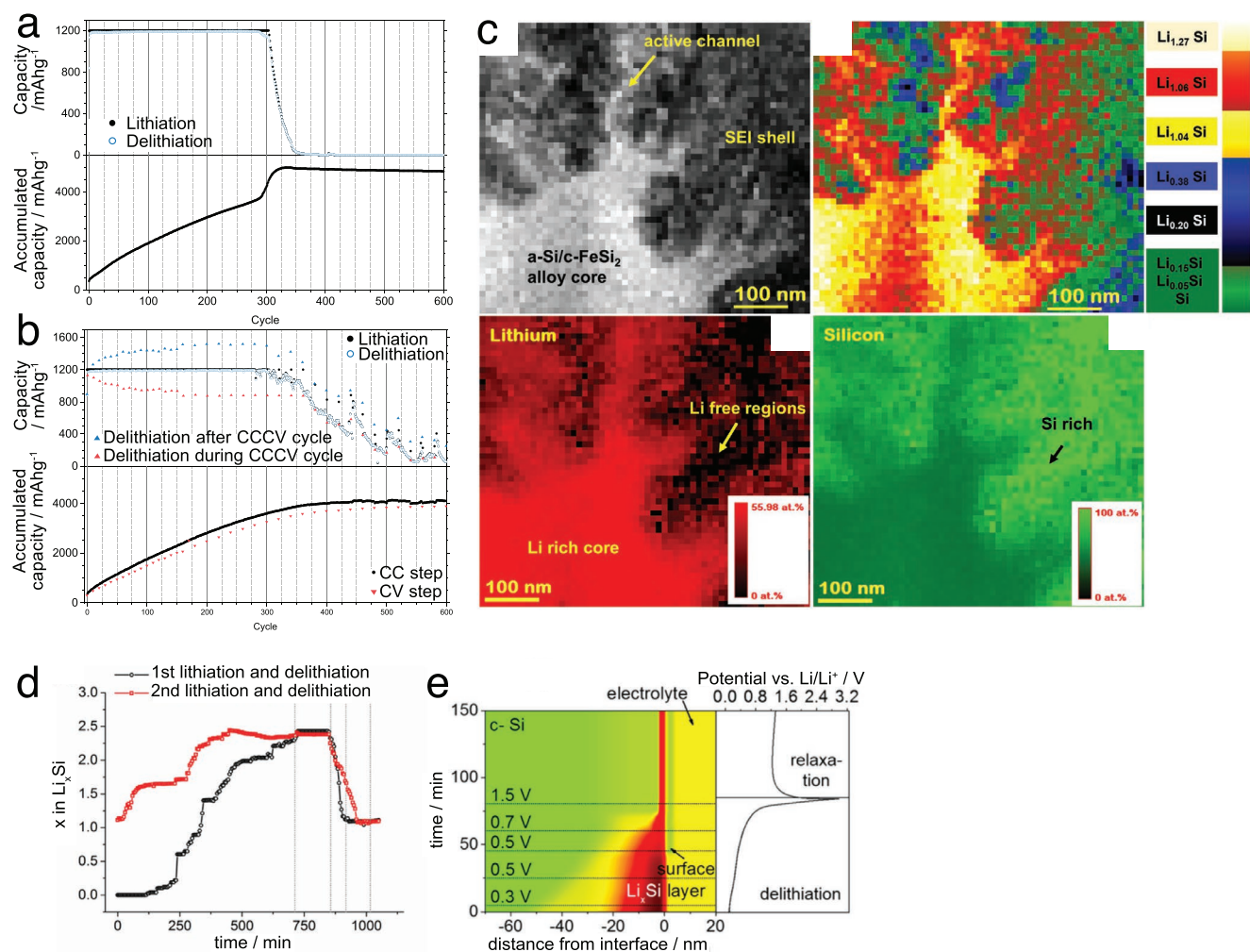


Figure 3. Capacity and accumulated capacity losses observed for nanosilicon composite electrodes using a) constant current cycling (i.e., CC) cycling and b) constant current followed by constant voltage (i.e., CCCV) cycling. Reproduced with permission.^[20] Copyright 2019, Wiley-VCH. c) Determination of residual Li_xSi and Li-trapping in a delithiated Si-FeSi₂ particle after 700 cycles at a 1 C rate using low-loss annular dark-field (ADF) scanning tunneling electron microscopy with electron energy loss spectroscopy (STEM-EELS). Reproduced with permission.^[29] Copyright 2020, Wiley-VCH. d) Changes in the lithium content x in Li_xSi in the skin region during the first and second lithiation. e) Scattering length density (SLD) profiles for the first delithiation as a function of time, distance from interface, and potential of the working electrode versus Li⁺/Li. The depletion of Li is represented by a color change from yellow/red (Li_xSi) to green (Si). The black solid lines depict the exemplary SLD curves shown in panel (e). Reproduced with permission.^[88] Copyright 2016, American Chemical Society.

from the electrode so that the stored charge is irreversibly lost. This form of Li-trapping found in so called “dead Li” isolated Li metal structures and Li isolated in particles that no longer are in contact with the current collector, can be either thermodynamically or kinetically controlled. Reversible (kinetically controlled) Li-trapping can occur when Li-rich phases inside the host material become temporarily inaccessible due to the above-mentioned diffusion-controlled trapping effect. The degree of reversibility is then defined by the time domain available for Li-diffusion during the lithiation and delithiation steps. In this review we thus focus on the diffusion-controlled (reversible) Li-trapping effect.

3. Lithium-Trapping in Battery Materials and Components

3.1. Negative Electrode Materials

3.1.1. Alloy-Forming Materials

Silicon is considered to be one of the most promising negative electrode material for LIBs due to its high theoretical capacity, low working potential, and high natural abundance.^[9] The commercial use of silicon electrodes is, however, hindered by the significant capacity losses generally observed during the cycling of silicon electrodes. The capacity fading mechanism has been intensively studied and is generally believed to originate from the large volume changes of the Si particles during lithiation and delithiation in combination with an unstable SEI.^[9] A range of strategies aimed at minimizing the volume expansion effect have therefore been developed, employing, for example, nanostructured Si active materials and multifunctional binders.^[89,90] More robust SEIs have also been designed by introducing electrolyte additives such as FEC and vinylene carbonate, as well as by replacing the traditional LiPF₆ salt with LiTFSI and LiFSI.^[20] Significant capacity losses during cycling are, however, still observed even when using the abovementioned optimization strategies. This raises the question whether the remaining stability issues can be explained by diffusion-controlled trapping of elemental lithium.

Lindgren et al.^[20] studied the capacity fading mechanisms of electrodes composed of Si nanoparticle using experimental conditions designed to address the typically proposed fading mechanisms, that is, volume expansion and SEI formation. The electrodes, which were used together with functional binders, an LiTFSI electrolyte and SEI stabilizing electrolyte additives (i.e., vinylene carbonate and FEC), were studied in half-cells using capacity limiting cycling. It was found that the Si electrode was able to maintain the set capacity of 1200 mAh g⁻¹ for about 300 cycles after which a capacity loss to virtually zero was observed during 50 cycles (Figure 3a). This dramatic capacity drop was unexpected as Coulombic limited cycling protocols have been reported to improve the cycling stability of Si anodes.^[91] Lindgren et al.,^[20] however, also used a modified cycling protocol in which a constant voltage delithiation step was included after the constant current step (i.e., to yield a CCCV protocol) on every tenth cycle, as is seen in Figure 3b. These constant voltage Li extraction steps not only

increased the delithiation degree of the electrode but also increased the cycling stability significantly (Figure 3b). As the CCCV delithiation steps decreased the accumulated capacity loss it was concluded that the main part of the capacity loss was due to diffusion-controlled Li-trapping, in good agreement with previous findings.^[28] The abovementioned results consequently indicate that it is possible to retrieve some of the trapped Li (and hence some of the lost capacity) if the efficiency of the delithiation step is increased. Chen et al.^[92] investigated the cycling stability of a Si electrode in a solid-state Si-Li₃PO₄-LiCoO₂ microbattery by studying the lithium distribution in the full-cell using neutron depth profiling (NDP). Lithium immobilization in Si phases protruding into the solid-state electrolyte was found to be the main source of the capacity loss. The accumulation and trapping of Li in the Si electrode resulted in an overall decrease in the capacity of the LiCoO₂ cathode. At the end of life, the cell was exposed to a CCCV step which showed a significant capacity increase, that is, about 10% of total the full-cell capacity when comparing to the first cycle discharge capacity.

In an attempt to understand the capacity loss mechanisms, Lee et al.^[93] used a calculation method to distinguish capacity losses based on irreversible electrolyte decomposition from those caused by Li-trapping. The model was based on the determination of the alloy charge (Q_{alloy}) on each cycle by comparing galvanostatic intermittent titration technique (GITT) cycling data with data based on reference galvanostatic lithiation profiles. Using this approach, the authors discovered that the capacity decay was mainly caused by Li-trapping, except during the first few cycles when there was also a contribution from electrolyte decomposition (i.e., SEI formation). Kumar et al.^[29] investigated the cycling stability of a Si-FeSi₂ nano-architected composite electrode by using advanced electron microscopy in combination with electrochemical analyses. Due to repeated volume fluctuations of the amorphous silicon phase during the cycling, the Si-FeSi₂ alloy was transformed from a core-shell structure into a tree-branch structure. After over 700 cycles, a dramatic capacity decay was seen, and the electrode was subjected to post-mortem scanning tunneling electron microscopy with electron energy loss spectroscopy (STEM-EELS) analysis. The elemental mapping of Li and Si showed the presence of significant amounts of Li within the Si host material, as can be seen in Figure 3c. Progressive Li-trapping gave rise to an enrichment of Li in the core of the Si host corresponding to a composition of Li_{1.27}Si. This effect, albeit less pronounced, is in good agreement with the previously mentioned^[20] enrichment yielding a lithium-to-silicon atomic ratio of 3.28 (i.e., Li_{3.28}Si). In the latter case, the lithium concentration was determined in an extensively cycled nano-Si composite electrode using inductively coupled plasma-atomic emission spectroscopy (ICP-AES) post-mortem analysis. The diffusion-controlled trapped Li could explain 80% of the accumulated capacity loss while the remaining 20% was ascribed to the charge associated with SEI formation and SEI dissolution.^[20] The enrichment of lithium in silicon electrodes clearly indicates that the diffusion-controlled trapping of Li can be readily detected after extended cycling. As will be explained below, indications of such Li-trapping can, however, also be found during the first cycles when employing in situ or operando techniques.

Seidlhofer et al.^[88] took advantage of the strong scattering contrast between Li and Si in in operando neutron reflectivity to monitor the Li uptake and release in a single crystal Si electrode. It was found that the uptake of Li during the first lithiation process resulted in a Li-rich lithiation phase ($\approx\text{Li}_{2.5}\text{Si}$) on the surface and a less lithiated zone ($\approx\text{Li}_{0.1}\text{Si}$) deeper within the crystal (Figure 3d). In addition, the difference between the profiles for first and second cycles clearly indicated the presence of a Li-trapping effect. During the second lithiation step, the residual Li phase resulted in a premature Li saturation of the Si electrode. As can be seen in Figure 3e, a surface layer of lithium in fact remained within the silicon electrode even after an 85-min long delithiation step at 1.5 V. These results thus indicate that Li was trapped during the first cycle due to an incomplete delithiation step and that this phenomenon affected the lithiation on the subsequent cycles. Pereira-Nabais et al.^[94] studied the lithium distribution in thin Si films during the initial cycles using time-of-flight secondary ion mass spectrometry (ToF-SIMS). The elemental composition and species distribution in the Si electrode were studied and used to determine the chemical origin and distribution of the detected Li species in the SEI and Si electrode, respectively. In the Li profile for the first delithiation step, Li peaks were discovered both at the electrode/electrolyte interface and the electrode/current collector interface. This hence indicate that the lithium in the electrode diffused both toward the electrode surface and toward the current collector during the delithiation step, in accordance with the previously mentioned two-way diffusion model.^[28] To study the distribution of the trapped lithium in the silicon, the same group^[95] developed ToF-SIMS chemical mapping methods involving in situ focused ion beam cross-sectional analyses of delithiated Si composite electrodes after five and ten cycles. An increased residual Li content was detected in the Si particles indicating progressive lithium trapping during the cycling.

Yoon et al.^[22] studied the capacity fading mechanism of Si nanoparticle composite electrodes by determining the capacity in different potential regions during the lithiation. The total capacity decrease was found to coincide with the capacity decrease during the early stages of the lithiation (i.e., between 0.8 and 0.27 V vs Li^+/Li). As the lithiation was gradually shifted to lower potentials, the lithiation time (and hence the lithiation capacity) decreased as the set potential cut-off was reached earlier and earlier. This behavior can be explained by the fact that the equilibrium lithium deposition potential should be shifted to lower potentials when the Li concentration (or rather the Li activity) in the Si electrode increases due to Li trapping.^[20,29] Moreover, as the activity of Li in the pristine Si electrode should be very low, the initial Li-deposition should in fact take place at a potential significantly more positive than 0 V versus Li^+/Li . In addition, the diffusion rate of Li in the silicon would be expected to decrease as the concentration of Li in the silicon electrode increases. Due to these two effects, the preset cut-off would hence be reached earlier and earlier during a controlled current experiment, which means that the capacity would become lower and lower during the cycling.^[20,29] Lindgren et al.,^[20] however, showed that the influence of these effects can be decreased by increasing the efficiency of the delithiation step using a CCCV delithiation protocol. As this delithiation approach resulted in a decrease in the surface concentration of

Li in the Si electrode, some lithiation capacity could be maintained during many additional cycles (Figure 3a,b). This consequently means that the potential shifts seen during the lithiation of Si can mainly be explained by the diffusion-controlled Li-trapping altering the electrochemical lithiation potential and the Li diffusion rate in the electrode.

Tin is another interesting negative electrode material which can store charge both via the conversion of tin oxides to yield tin and Li_2O (e.g., $\text{SnO}_2 + 4 \text{Li}^+ + 4 \text{e}^- = \text{Sn} + 2 \text{Li}_2\text{O}$) and the lithiation of the generated tin (e.g., $\text{Sn} + 4.4 \text{Li}^+ + 4.4 \text{e}^- = \text{Li}_{4.4}\text{Sn}$). Although reversible $\text{Li}_{4.4}\text{Sn}$ alloy formation offers a theoretical capacity of 999 mAh g^{-1} , poor cycling stability is generally seen. In analogy with silicon, the latter is typically ascribed to the considerable volume expansion (i.e., 244%) associated with the lithiation.^[9] The use of electrodes composed of nanometer-sized particles has, however, been found to yield more mechanically stable electrodes in good agreement with corresponding results for Si electrodes. As capacity decays nonetheless are commonly observed for nano-Sn electrodes it is reasonable to assume that there is at least one other phenomenon affecting their cycling stabilities. Rehnlund et al.^[28] showed that diffusion-controlled Li-trapping can explain the capacity decay seen for Sn nanorod electrodes. In this case, the decay was seen after an initial capacity increase which was ascribed to an increase in the surface area of the electrode due to volume expansion effects. The Sn nanorod electrodes were cycled either between 2.5 and 0.1 V (vs Li^+/Li), or between 1 and 0.1 V (vs Li^+/Li), using cyclic voltammetry (CV) at a scan rate of 1 mV s^{-1} (Figure 4a–c). An improved cycling performance was observed when 1 V (vs Li^+/Li) was used as the upper potential limit which could be explained by the difference in the scan time associated with scanning to 1 or 2.5 V. The latter was shown by determining the capacities after stopping the scan at 1 V on each oxidation step for time corresponding to the scan time from 1 to 2.5 V and back. As the observed capacity decrease was analogous to that seen when scanning to 2.5 V and no electrochemical reactions that could explain the loss of capacity were observed in the 1–2.5 V range, it was concluded that the size of the capacity loss depended on the time domain of the experiment. ICP-AES analyses of delithiated Sn nanorod electrodes (Figure 4d) clearly showed that the amount of Li found in the delithiated electrode depended linearly on the cycle number. It should also be mentioned that a plot of the capacity as a function of the square root of the time was found to be linear in the region where a capacity loss was seen, indicating that the capacity loss was caused by a diffusion-controlled process. It was hence concluded that the capacity decay seen for the Sn nanorod electrodes mainly was due to progressive Li-trapping caused by a two-way diffusion phenomenon.^[28]

Co and coworkers^[96] employed in situ NDP to study the distribution of Li in Sn thin foil negative electrodes. Increases and decreases in the Li concentration were observed during the lithiation and delithiation steps with faster delithiation taking place at the Sn/electrolyte interface compared to in the bulk of the electrode. After one cycle, a considerable amount of Li hence remained in the bulk, and the Li then diffused deeper into the electrode toward the current collector when the cell was paused at the open-circuit potential. This finding shows that there was diffusion of Li in the electrode as the Li concentration was

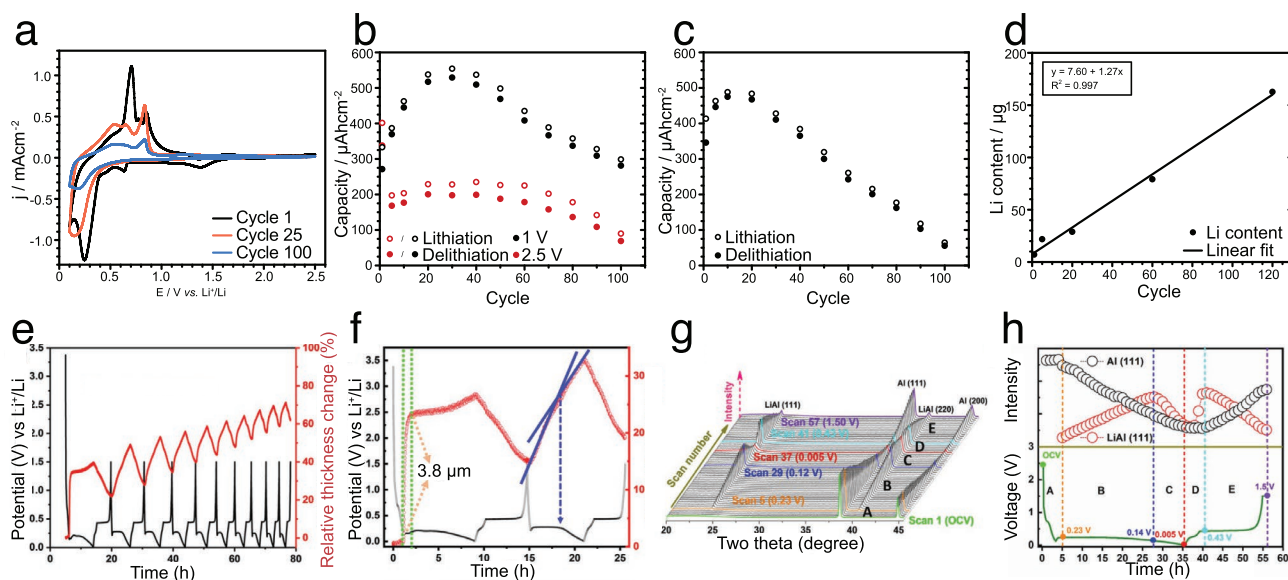


Figure 4. a) Cyclic voltammograms obtained with Sn nanorod electrodes showing the 1st, 25th, and 100th cycle when scanning between 0.1 and 2.5 V (versus Li^+/Li) at a scan rate of 1.0 mV s^{-1} . b) Areal lithiation (open circles) and delithiation (filled circles) capacities as a function of the cycle number for CV cycling between 0.1 and 1.0 V (black symbols) and 0.1 and 2.5 V (red symbols), respectively. c) Areal capacities for CV cycling between 0.1 and 1.0 V with a 3000 s long pause at 1.0 V on each cycle. The length of the pause corresponded to the time needed to cycle from 1.0 to 2.5 V and back at 1.0 mV s^{-1} . d) The Li amount found in delithiated Sn nanorod electrodes as a function of the scan number. The Li amounts were determined using ICP-AES after CV cycling between 0.1 and 2.5 V. a–d) Reproduced with permission.^[28] Copyright 2017, The Royal Society of Chemistry. e) Displacement profile and corresponding cycling curve for an Al composite electrode obtained using in situ electrochemical dilatometry with f) magnified electrode displacement and cycling curve showing the first 1.5 cycles. g) In situ X-ray diffraction (XRD) data for the Al electrode during the first cycle with h) the corresponding cycling curve together with the XRD intensity variations of the Al (111) and LiAl (111) reflections. e–h) Reproduced with permission.^[33] Copyright 2019, Wiley-VCH.

significantly higher at the electrode surface than in the rest of the electrode after the lithiation step. It is, however, important to note that as the delithiation step was significantly shorter than the lithiation step (i.e., 200 vs 740 min), the interpretation of these results is less straightforward. The asymmetric cycling should clearly have resulted in an incomplete delithiation, even though the lithiation rate has been found to be lower than the delithiation rate for Si electrodes.^[20,86] Such an asymmetric behavior (which appears to be caused by the concentration gradients of Li (or Li^+) generated in the electrode material) has, incidentally, also been seen for TiO_2 .

Li et al.^[97] reported that Li-trapping gave rise to capacity losses for nanosized SnSb alloy electrodes. The reversibility of the binary alloy was found to depend on the alloy composition since the behavior of the Li-Sn alloy was more reversible than that of the Li-Sb alloy. In the presence of preferential Li-trapping in one of the elements in an alloy, a Li-trapping effect may hence affect the properties of an alloy-based electrode in an unexpected manner. While the use of a binary alloy may improve the mechanical stability of an electrode, the electrochemical performance can, on the other hand, be decreased by preferential lithiation. When discussing Li-trapping in metals, it should also be mentioned that the effect should involve elemental Li rather than Li^+ , as lithium ions (for obvious electro-neutrality reasons) cannot diffuse into a metal in the absence of a counter ion.^[36]

Aluminum is an alloy forming negative electrode material that has attracted far less interest than silicon, despite its low cost, large natural abundance, and small volume expansion

effect (i.e., 90% for LiAl compared to 280% for $\text{Li}_{15}\text{Si}_4$).^[9] As the fully lithiated LiAl phase offers a theoretical capacity of 933 mAh g^{-1} , aluminum electrodes could, nevertheless, be alternatives to commercial graphite negative electrodes. In analogy with silicon, aluminum is, however, known to exhibit poor cycling stability. The capacity loss is typically ascribed to volume expansion effects, despite the fact that these are relatively small for aluminum. Oltean et al.^[35] came to question this hypothesis when studying the capacity decay of binder-free Al nanostructured electrodes synthesized by template-assisted electrodeposition. Using Al nanorods which were fortified with Al_2O_3 layers with a thickness up to 60 nm, no correlation was found between the cycling stability and the thickness of the (mechanically stabilizing) alumina layer. Post-mortem SEM analyses also showed that the Al nanorods remained well connected to the substrate after the cycling experiments. In addition, the authors found that the capacity decayed with time in a manner which was unlikely to stem from volume expansion and/or SEI effects. The capacity losses were instead ascribed to diffusion-controlled trapping of Li in the aluminum nanorods as a result of a two-way diffusion process. This hypothesis was subsequently investigated in more detail using Sn and Si electrodes.^[20,28]

Qin et al.^[33] carried out a systematic investigation of the Li-alloy formation process for Al electrodes by employing in situ X-ray diffraction (XRD), electrochemical dilatometry, X-ray photoelectron spectroscopy (XPS), as well as in operando isothermal microcalorimetry. It was found that both the lithiation and delithiation were incomplete as well as asymmetric and that

this gave rise to the growth of an residual Li_{1-x}Al phase in the bulk of the electrode, in good agreement with previous findings of Liu and Co using NDP.^[32] Moreover, by studying the volume fluctuations of the cell during operation with electrochemical dilatometry Qin et al.^[33] demonstrated a gradual increase in the electrode displacement (Figure 4e). This effect, which could be seen already after one cycle, suggested an incomplete delithiation and hence the presence of trapped Li in the Al electrode (Figure 4f). Employing in situ XRD, the authors observed an increase and decrease in the Li_xAl intensity during the lithiation and delithiation as well as a residual Li_{1-x}Al phase remaining in the structure after delithiation (Figure 4g,h). Residual LiAl was also detected by ex situ XPS, thereby supporting the hypothesis that Li-trapping can yield capacity losses for Al electrodes.

Lithium trapping in Al electrodes has also been demonstrated using real-time SEM imaging and Auger spectroscopy during electrochemical cycling of a solid-state Li-ion battery.^[98] The trapping, which resulted in a 90% loss of capacity during 100 cycles, was proposed to take place in the electronically conducting Al-Li alloy mounds irreversibly generated on the Al surface as a result of the formation of a stable Al-Li-O alloy.^[98] Such a layer has also been suggested to give decreased capacities and cycling stabilities when decreasing the thickness of the aluminum layer.^[34] The latter is in contrast to the general behavior of other Li-alloy electrodes since an improved specific capacity and cycling performance typically are seen when the film thickness or particle size is decreased to the submicron level.^[99] It should, however, be pointed out that Oltean et al.^[35] demonstrated that the electrochemical behavior of Al nanorods coated with a 60 nm thick Al_2O_3 surface was very similar to that seen for the corresponding nanorods with a native Al_2O_3 layer.^[35] The latter indicates that the Al_2O_3 layer mainly acted as a solid electrolyte and that the observed capacity loss was caused by the Li-trapping phenomenon discussed above.

3.1.2. Intercalation Materials

Carbonaceous materials constitute a large family of negative electrode materials, with crystalline graphite being the commercial standard for LIBs.^[1] While there is a multitude of different carbon electrode materials with varying degrees of structural ordering, carbon materials are often divided into graphitized, non-graphitized, and intermediate materials.^[100] In this report, we will mainly discuss ordered (i.e., graphite and soft carbon) and disordered (i.e., hard carbon) carbon materials, exhibiting long-range and short-range order, respectively. Like other negative electrode materials, carbon materials exhibit a significant irreversible capacity loss on the first cycle which generally is ascribed to the formation of an SEI layer.^[101] Apart from this initial capacity drop, carbon electrodes typically exhibit very good cycling stabilities with small capacity decays under mild cycling conditions (i.e., at room temperature using low current densities). However, a decrease in the capacity can, nevertheless, still be seen also for carbon electrodes. Given that intercalation-based negative electrodes (e.g., carbon electrodes) generally exhibit small volume expansion effects, this capacity loss is less likely to be fully explained by volume expansion effects and/or SEI formation (especially when Li-metal half-cells are used).

In this section, we will therefore re-examine results obtained with carbon-based negative electrodes based on the diffusion-controlled Li-trapping hypothesis.

Matadi et al.^[47] conducted a thorough study focusing on the irreversible capacity losses of half-cells and commercial graphite/lithium nickel manganese cobalt oxide (NMC) cells containing Li metal reference electrodes under low temperature cycling conditions (i.e., 5 °C). By cycling the full-cell between 0% and 100% SOC, a continuous capacity decay was observed yielding a 75% capacity loss after only 50 cycles. During this time, the end of charge (lithiation) graphite electrode potential decreased toward 0 V versus Li⁺/Li. Post-mortem XRD results indicated that Li⁺ was present in the graphite electrode even after delithiation (see Figure 5a). This was further confirmed by ⁷Li nuclear magnetic resonance (NMR) results (see Figure 5b) and visual observations of the brown graphite electrode surface indicating the presence of LiC_x . The authors concluded that the capacity decay mainly stemmed from Li⁺-trapping in the graphite electrode due to an incomplete Li⁺ de-intercalation step caused by the presence of a layer of electrolyte degradation products on the surface of the electrode.

Yao et al.^[48] employed spatially resolved energy dispersive X-ray diffraction to study the formation of Li⁺ concentration gradients in graphite electrodes during their lithiation and delithiation. It was found that the lithium distribution was inhomogeneous with respect to both the total lithium content and the Li_xC_6 phases formed during the lithiation and delithiation steps. Moreover, the delithiation concentration profiles did not mirror the lithiation profile in reverse and this asymmetry was also found to become more pronounced deeper into the electrode. In the deepest layers, the LiC_6 and LiC_{12} phases were seen to persist much longer than in the surface layer. The experimental results were stated to indicate the presence of incomplete delithiation of the graphite and a risk of preferential Li plating in the Li-rich zone at the electrode surface.

Studies involving disordered carbon materials have indicated the presence of irreversible capacity losses which have been attributed to different lithium-consuming reactions.^[49–53] Matsumura et al.^[50] reported that a significant part of the irreversible capacity loss on the first cycle was due to the irreversible immobilization of Li species in the bulk of the electrode. This effect was studied using delithiated carbon electrodes and various analytical techniques including Fourier transform infrared attenuated total reflectance, secondary ion mass spectrometry, XPS, and determinations of the amounts of Li in the electrodes using plasma spectrometry. The results clearly showed that some Li remained on the surface and in the bulk of the discharged (i.e., delithiated) carbon electrode, with a significantly higher Li concentration in the surface layer compared to in the bulk. The Li concentration in the delithiated electrode was also much higher than in a pristine electrode. As the binding energy for the bulk Li species was 2.5 eV higher than for metallic Li it is reasonable to conclude that the Li species remaining in the bulk were intercalated Li-ions. The incomplete delithiation was ascribed to Li⁺ ions reacting with active sites within the electrode to yield compounds that could not undergo delithiation.^[50]

The results of a ⁷Li NMR study on lithiated hard carbon^[102] indicated the existence of two different lithium species in the internal porosity; quasi-metallic lithium aggregates and lithium

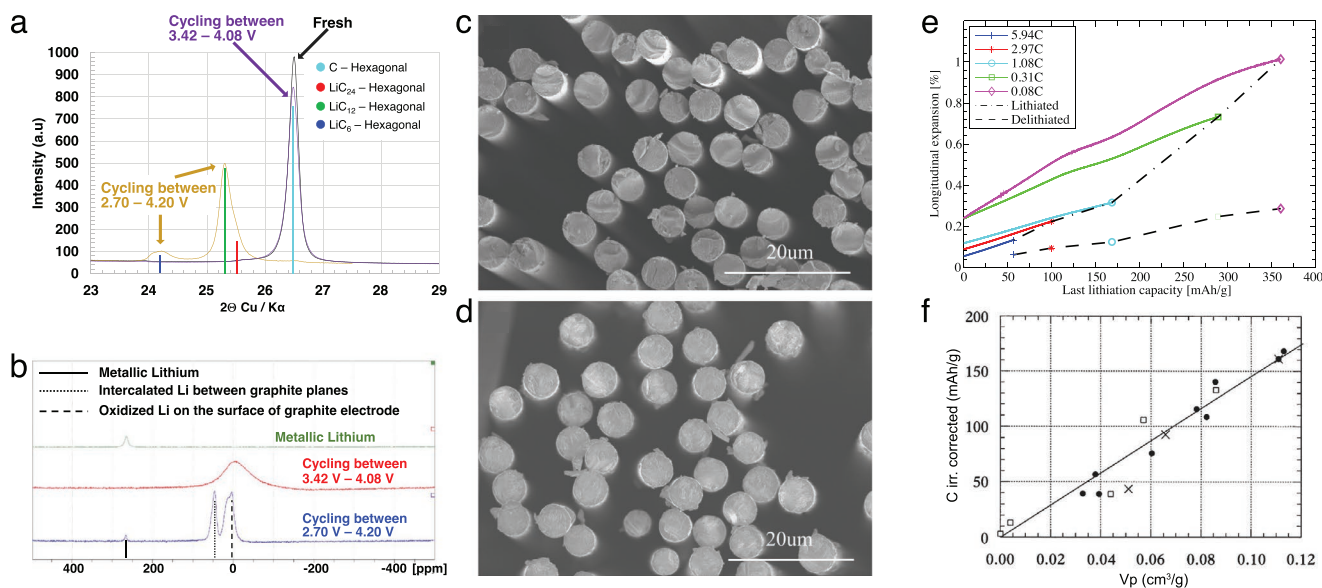


Figure 5. Post-mortem analyses of cycled graphite electrodes after cell failure (i.e., after 50 and 1500 cycles between 2.70 and 4.20 V as well as 3.42 and 4.30 V, respectively) probed in the delithiated state using a) XRD and b) ^7Li NMR. Reproduced with permission.^[47] Copyright 2017, ECS. Cross-sectional SEM images of c) pristine carbon fibers (CFs) d) and fully lithiated CFs. e) Longitudinal expansion of CFs with the capacity indicated for the last lithiation at the different C-rates. c–e) The difference between the total expansion of the lithiated CFs (dash-dot line) and the irreversible expansion of the CFs after the last delithiation (dashed line) shows the last cycle-reversible expansion at the different C-rates. Reproduced with permission.^[51] Copyright 2013, Elsevier. f) The irreversible capacity corrected for passivation and binder contributions as a function of the internal pore volume. Reproduced with permission.^[52] Copyright 2000, Elsevier.

covalently bound to the pore surface (at the edges of small crystallites) demonstrating the complexity associated with the interpretation of the hard carbon insertion process. Takami et al.^[54] performed an electrochemical analysis of the large hysteresis effect observed for disordered carbon electrodes. It was found that the Li^+ diffusion coefficient decreased dramatically during the lithiation step, and that the diffusion coefficient was lower during the delithiation step than during the initial part of the lithiation step. This asymmetry regarding the lithiation/delithiation process seems to be an inherent characteristic of negative electrode materials as analogous results have been obtained with Si electrodes.^[20,86]

Jacques et al.^[51] used an in situ electron microscopy technique to study the influence of the lithiation charge on the longitudinal expansion of carbon fibers (CFs). As shown in Figure 5c,d, distinct expansion could be seen for lithiated carbon fibers when compared to pristine carbon fibers. The expansion was almost linearly dependent on the lithiation capacity suggesting that the measured expansion was a result of the lithium intercalation and hence the amount of inserted lithium ions (see Figure 5e). The transverse expansion, estimated from cross-sectional SEMs, was between 8% and 13% for the fully lithiated carbon fibers, which is of the same order of magnitude as the increase in the interlayer spacing for lithium-ion intercalated graphite.^[103] After the delithiation step a significant expansion, however, still remained indicating that the delithiation of the carbon fibers was incomplete. This behavior, which is in good agreement with the Li^+ -trapping effect generally seen for carbon materials, hence shows that the effect also can affect the mechanical properties of carbon material.^[104] Guerin et al.,^[52] who conducted a study on hard carbon electrodes with low heteroatomic contents

and low specific surface areas, concluded that the irreversible capacity losses due to the surface area and surface functional groups were negligible. A linear relationship between the irreversible capacity loss and the internal pore volume of the electrode was, on the other hand, found (see Figure 5f) indicating that the irreversible capacity loss resulted from Li-trapping in the bulk of the electrode.

Metal oxides can also be used as negative electrode materials in LIBs since there is a large variety of transition metals that can store charge based on intercalation or conversion reactions. In this report focusing on diffusion-controlled Li-trapping, we will, however, only discuss intercalation reactions since the capacity losses seen for conversion materials mainly are due to other effects, such as the formation of passivating surface oxides during the delithiation (i.e., oxidation) of the metal nanoparticles generated in the conversion reaction (e.g., $\text{SnO}_2 + 4 \text{Li}^+ + 4 \text{e}^- = \text{Sn} + 2 \text{Li}_2\text{O}$).^[105–108] Diffusion-controlled Li-trapping effects should, nevertheless, still be possible to see for electrode materials undergoing conversion reactions providing that the capacity losses due to the abovementioned irreversible conversion reaction and the Li-trapping effects can be differentiated. The problem can be illustrated using SnO_2 as an example. During the oxidation of the Sn nanoparticles formed in the conversion reaction (see the reaction above), the Sn nanoparticles first become coated with a layer of SnO which acts as a passive layer and thus slows down the oxidation of the nanoparticles. Although the SnO layer can be further oxidized to yield a surface layer of SnO_2 on top of the SnO layer, it is difficult to fully regenerate the original SnO_2 particles. This inability to reform the original metal oxide particles would clearly give rise to a significant loss of capacity, the magnitude of which would depend on,

for example, the size of the metal oxide particles, the size of the generated nanoparticles, the nature of the oxide, the cycling rate, and the employed potential window. It would therefore not be straightforward to evaluate the capacity loss due to the Li-trapping in the Sn nanoparticles even if the cycling were conducted down to potentials where a Li_xSn alloy is formed. Due to this complication (and the fact that we are not aware of any studies involving materials undergoing conversion reactions exhibiting evidence of a diffusion-controlled conversion reaction) conversion-type electrode materials will not be further discussed here.

During an intercalation reaction, lithium ions are instead inserted into the material to maintain electroneutrality within the electrode material (e.g., $\text{TiO}_2 + x \text{Li}^+ + x \text{e}^- = \text{Li}_x\text{TiO}_2$). While the lithium ions are electroinactive counter ions, their presence in the delithiated metal oxide electrode can be used to detect capacity losses due to an incomplete delithiation of the electrode material. Wei et al.^[36] investigated the capacity limiting effects for binder- and additive-free monolithic TiO_2 nanotube electrodes. By comparing the results of galvanostatic and voltammetric experiments it was found that the capacity was limited by the lithiation step and that the lithiation capacity was limited by the Li^+ diffusion rate in the electrode. A diffusion-controlled Li^+ -trapping effect could also be seen at sufficiently high cycling rates particularly when an open circuit step was used between the lithiation and delithiation steps. The latter was explained based on the diffusion of Li^+ further into the TiO_2 material causing a

fraction of the capacity to become inaccessible during the subsequent delithiation step. In analogy with previous results for Si electrodes,^[20,86] an inherent asymmetry regarding the lithiation and delithiation rates was also observed favoring the delithiation step. The latter was explained on the fact that the lithiation should give rise to a decrease in the available Li-ion sites in the host structure (and hence a gradually decreasing diffusion coefficient) whereas an increase in the number of available Li-ion sites can be seen during the delithiation step.

Electroactive metal oxides such as WO_3 and NiO are particularly interesting in the present context as the insertion/extraction of Li^+ in these materials also give rise to changes in the optical properties of the materials.^[109,110] Upon cycling of these materials irreversible capacity losses and gradually declining optical responses are generally seen, which typically are ascribed to a lithium-ion trapping effect.^[56,111,112] **Figure 6** shows the electrochemical and electrochromic performance of X-ray amorphous WO_3 thin films cycled in an electrolyte composed of 1 M LiClO_4 in propylene carbonate. It is immediately evident that the charge capacity as well as the optical transmittance decreased during the voltammetric cycling. This was ascribed to an accumulation of Li-ions in the WO_3 electrode, that is, Li^+ -trapping in three main types of traps. It should, however, be noted that potential interferences from the WO_3 conversion reaction generally appear to have been neglected in these electrochromic studies. Diao and coworkers^[55] likewise concluded

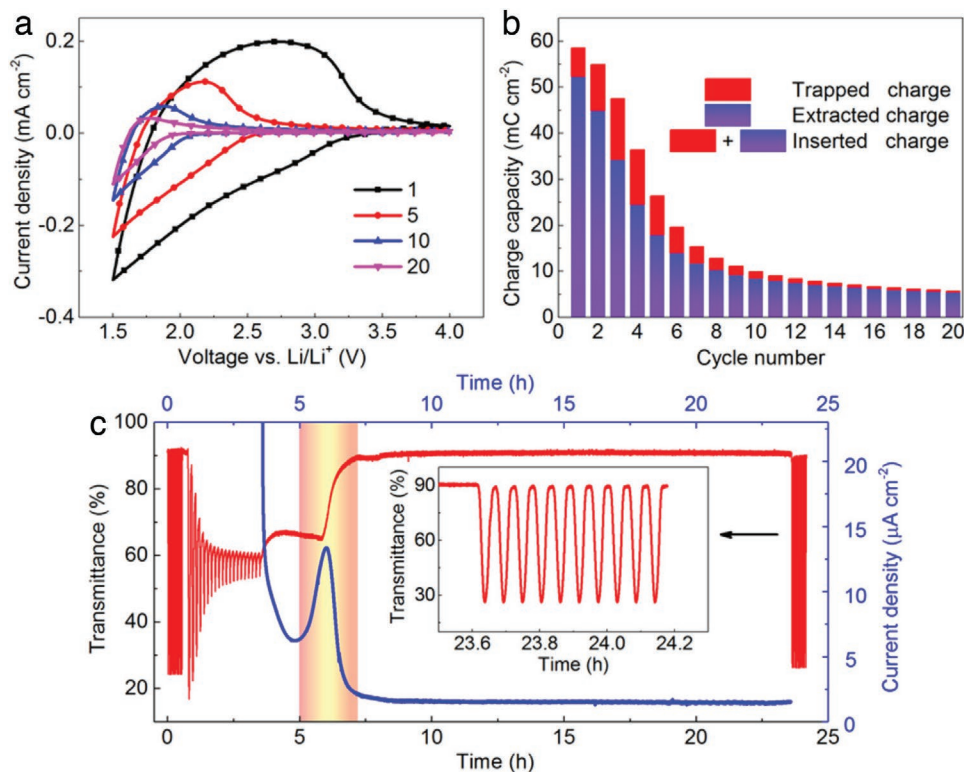


Figure 6. Electrochemical and electrochromic performance of $\approx 300 \text{ nm}$ thick amorphous WO_3 films. a) Cyclic voltammograms recorded between 1.5 and 4.0 V versus Li^+/Li at a scan rate of 10 mV s^{-1} for the indicated cycles. b) Charge capacity as a function of the cycle number featuring the inserted, extracted, and trapped charges. c) In situ optical transmittance measured at a wavelength of 550 nm and current density as a function of time for potentiostatic Li^+ extraction at 5.5 V. The inset shows the transmittance as a function of time for the indicated time window. Reproduced with permission.^[111] Copyright 2016, American Chemical Society.

that the degradation of cycled all-solid-state WO_3/NiO electrochromic devices was caused by lithium ion-trapping. The latter authors observed a significant increase in the thickness of cycled WO_3 thin-film electrodes, indicating an irreversible insertion of Li^+ . A combined XPS and ToF-SIMS analysis of the WO_3 -NiO electrochromic devices revealed a progressively increasing residual Li^+ concentration inside the metal oxide films during cycling, in agreement with previous findings for WO_3 thin films.^[112] An analysis of the XPS results suggested that the lithium ions were trapped at different types of sites within the material. Rejuvenation of degraded electrochromic films was, however, possible via extraction of trapped Li-ions using extended constant current or potentiostatic delithiation.^[56,113] Since a fraction of lithium ions typically remains in the films, a complete rejuvenation has so far been difficult to achieve.^[112]

3.2. Positive Electrode Materials

There are, so far, few reports discussing capacity losses due to diffusion-controlled Li-trapping in positive electrode materials. This is somewhat surprising since most positive electrode materials in analogy with many negative electrode materials are Li^+ intercalation or insertion materials. It is therefore reasonable to assume that diffusion-controlled Li-trapping likewise can affect the performance of many positive electrode materials. Some experimental results supporting this hypothesis are described below.

LFP is a commonly used positive electrode Li^+ -insertion material in LIBs.^[114] However, LFP-based electrodes rarely reach their theoretical capacities even at low current densities and elevated temperatures^[115] due to the relative low rates of the Li^+ extraction and insertion processes. The first cycle performance of LFP electrodes was studied by Andersson and Thomas^[38] using NDP. It was suggested that the lithium ions could not be fully extracted from the LFP particles, indicating that the electrode could not be fully oxidized, and that this resulted in a trapping of about 20% of the lithium ions. This effect, which gave rise to an initial capacity loss, was ascribed to sluggish lithium-ion diffusion and a low electronic conductivity in the delithiated phase based on the proposed formation of a lithium-rich core within the larger delithiated LFP particles. While investigating the cycling performance of LFP electrodes in half-cells containing functionalized separators, Pan et al.^[39] recently discovered a mass transfer dependent memory effect analogous to the diffusion-controlled Li-trapping effect seen for Li^+ insertion in TiO_2 nanotube electrodes.^[36] In both cases, the capacity was found to gradually decrease during cycling at rates of 5C and 10C although the full capacity was regained once the cycling was continued at a lower rate.

Marcus and colleagues have studied the lithium distribution and chemical composition in cycled thin-film electrodes containing V_2O_5 ^[43,116] and MoO_3 ^[45] using a combination of XPS, ToF-SIMS, and Rutherford Backscattering Spectrometry. XPS analyses of V_2O_5 electrodes after the first and second voltammetric cycles showed that the Li^+ extraction reaction was incomplete as 14 at% V^{4+} could still be found after de-intercalation at 3.8 V versus Li^+/Li .^[43] After 300 cycles, 17–22 at% of V^{4+} was observed at the V_2O_5 surface of the de-intercalated samples.^[116] Li and V depth profiles were generated with ToF-SIMS

to obtain the depth distribution of Li^+ in de-intercalated samples. As shown in **Figure 7a**, traces of Li^+ were found both at the electrode/electrolyte interface and in the bulk of the electrode. By comparing the Li and V bulk peaks obtained after 12 and 300 cycles, it could be seen that the Li-rich zone not only grew in size but also moved deeper into the electrode bulk during the cycling.^[43] These results, which indicate the presence of a Li^+ -trapping effect, show that the degree of de-intercalation (and hence the capacity) of the electrode decreased during the cycling. In addition, the results clearly demonstrate that there was diffusion of Li^+ in the electrode material due to the presence of Li^+ concentration gradients. As a result, Li^+ was also found in the non-electrochemically treated surface areas of the de-intercalated V_2O_5 samples. It is therefore reasonable to assume that the observed Li^+ -trapping effect was linked to Li^+ solid state diffusion. Analogous results were also obtained with $\text{V}_2\text{O}_5/\text{FTO}$ film electrodes.^[41] For MoO_3 thin-film electrodes, a large fraction of Mo^{5+} (i.e., 40%) was still found after de-intercalation at 3.2 V versus Li^+/Li indicating that Li-ions were trapped in the MoO_3 material.^[45]

Winter and coworkers^[117] studied the origin of the first cycle capacity losses observed for common positive electrode materials using electrochemical cycling combined with ICP-AES determinations of the lithium contents of the cycled electrodes. For $\text{LiNi}_{1/3}\text{Co}_{1/3}\text{Mn}_{1/3}\text{O}_2$ (i.e., NCM111), it was shown that about 70% of the specific capacity loss was associated with the limited rate of the lithiation reaction during the discharge (this part was denoted the recoverable capacity loss) whereas the remaining 30% was ascribed to irreversible structural changes leading to inactive domains inside the electrode material. The capacity loss due to the oxidation of the electrolyte was, on the other hand, found to be negligible. By limiting the pathways for Li^+ solid state diffusion by going from a 3D network to a 1D channel, the degree of recoverable capacity losses could be increased. This suggests that lithium-ion diffusion focused to single channels can give rise to lower irreversible capacity losses than diffusion in 3D. The irreversible capacity losses should hence be more pronounced for 3D materials such as $\text{LiNi}_{0.5}\text{Mn}_{1.5}\text{O}_2$ than for 1D positive electrode materials such as LFP. Winter and coworkers^[40] subsequently addressed the underlying cause of the capacity fading of NCM111 employing Li-metal-based half-cells. It was shown that the delithiation of the NCM111 was incomplete and that the influences of transition metal dissolution and CEI formation on the capacity loss were negligible. As can be seen in **Figure 7b,c**, both the charge (i.e., delithiation) and discharge (i.e., lithiation) capacities depended on the employed current densities. The charge capacities were, however, found to differ from the discharge capacities when the discharge current density was increased, hence yielding a capacity loss. Although an impeded relithiation reaction could explain the results obtained when increasing the lithiation current density, it could not explain the gradual capacity fade seen during constant current cycling. The latter effect was found to be more compatible with an increasingly delithiation limited reaction as a result of changes in the active material. It should also be mentioned that the results presented by Winter and coworkers^[40,117] clearly show that the capacity losses could be decreased significantly by using controlled potential steps after the controlled current delithiation and lithiation steps (i.e., CCCV cycling). This is important as it indicates that some of the

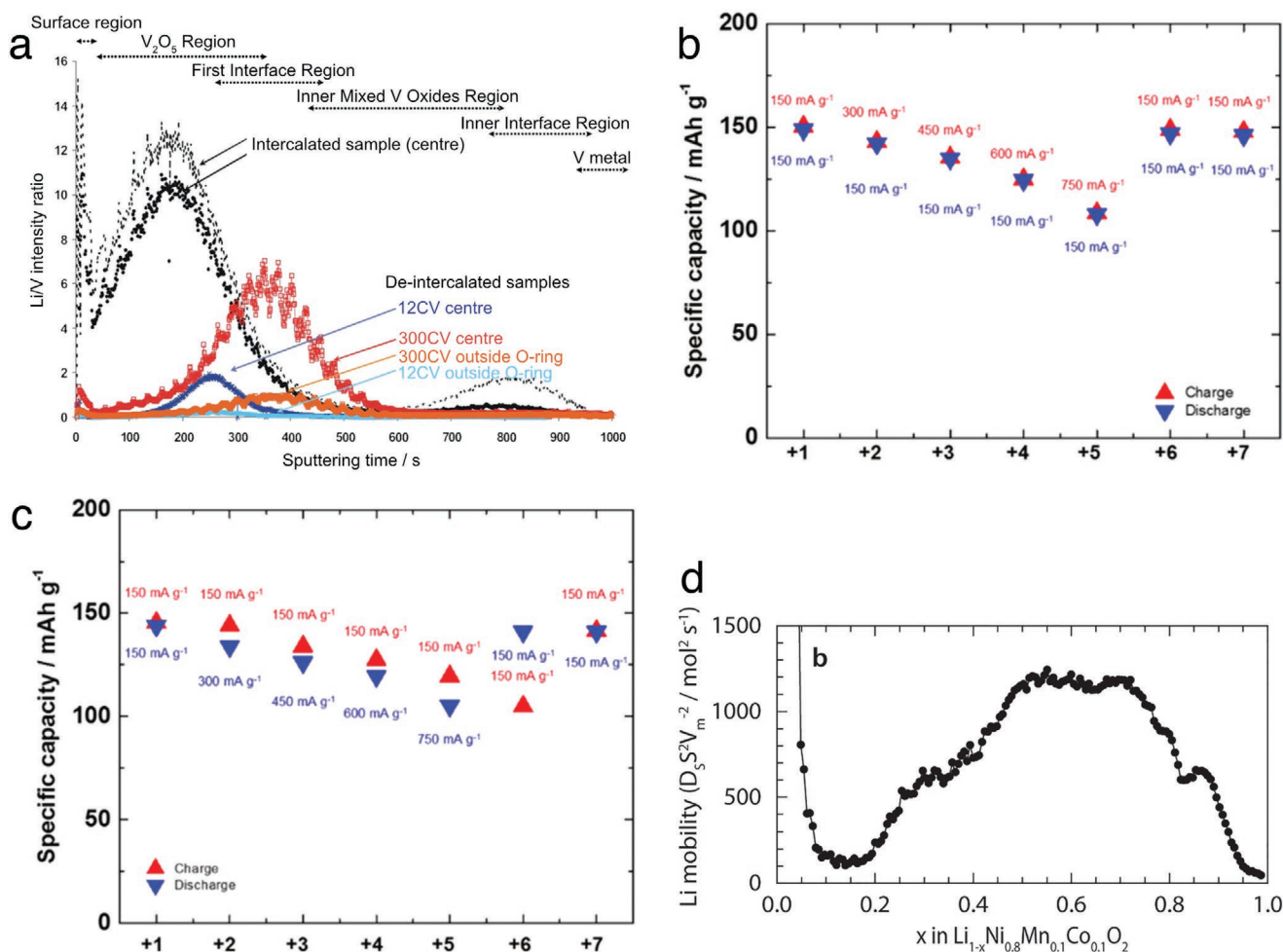


Figure 7. a) ToF-SIMS Li/V depth profiles obtained for V₂O₅/V films after intercalation at 2.8 V as well as after de-intercalation at 3.8 V after 12 and 300 cycles, respectively. Reproduced with permission.^[116] Copyright 2008, Elsevier. Specific capacity as a function of the cycle number for specific current density ranging from 150 to 750 mA g⁻¹ for the b) charge (i.e., delithiation) and c) discharge (i.e., lithiation) of LiNi_{1/3}Co_{1/3}Mn_{1/3}O₂ (NCM111) in NCM111/Li half-cells. Reproduced with permission.^[40] Copyright 2017, American Chemical Society. d) Change in the Li diffusion coefficient as a function of state-of-charge (SOC) for Li_{1-x}Ni_{0.8}Mn_{0.1}Co_{0.1}O₂ (NMC811) in NMC811/Li half-cells, as measured using the galvanostatic intermittent titration technique (GITT). Reproduced with permission.^[80] Copyright 2017, American Chemical Society.

lost capacity could be recovered by extending the time domain of the delithiation and lithiation steps. The latter is in good agreement with previous results obtained for negative electrode materials such as Si^[20] and TiO₂.^[36]

Grey and colleagues investigated the Li diffusion behavior inside Ni-rich Li_{1-x}Ni_{0.8}Mn_{0.1}Co_{0.1}O₂ (NMC811) cathode materials during cycling.^[79,80] Using a combination of in operando NMR and the GITT, the authors found that the Li diffusion coefficient was changed dramatically during the delithiation (as shown in Figure 7d). The Li extraction was initially slow but became increasingly faster in the SOC region 0.25–0.75, after which a dramatic drop in the Li diffusion coefficient was observed. The reduced Li diffusion rate at high SOC (i.e., above 0.75) was found to be caused by surface restructuring as a growing oxygen-depleted layer induced a lattice mismatch between the bulk and surface layer of the NMC811 electrode material. This resistive surface film hindered complete Li extraction thereby causing continuous capacity losses, as confirmed by operando XRD showing a growing “fatigued” lithiated

phase (i.e., Li_{0.26}Ni_{0.8}Mn_{0.1}Co_{0.1}O₂) formed inside the bulk during long-term cycling.^[79,85] The capacity decay was, however, partially reversible, and responsive to the cycling rate where at C/50 cycling rates extensively cycled cells behaved like pre-cycled cells. Asymmetric cycling with slow lithiation has also been shown to improve the cycling stability by allowing more time for Li-ions to diffuse into the bulk.^[118] It would therefore seem that the surface restructuring observed on Ni-rich cathodes induces a kinetic limitation to Li diffusion rate that quickly becomes rate limiting during extended cycling.

3.3. Current Collectors

Current collectors are important components in lithium-based batteries as they typically serve both as substrates for the electrode materials and electrical contacts. Based on the binary phase diagrams, copper,^[119] nickel,^[120] and titanium^[121] are generally assumed to be good current collectors for the negative

electrode since these metals do not form intermetallic alloys with Li under normal battery cycling conditions. Rehnlund et al.,^[28] however, showed that Li diffused into nickel, copper, and titanium pieces exposed to lithium metal at 50 °C for 7 days. Although the amounts of Li found in the metals merely were of the order of 10 μg and no attempts were made to try to recover the Li from the metal pieces, the results indicated that this diffusion likewise could give rise to a Li-trapping effect. The latter could give rise to a capacity loss, particularly when considering the relatively large volume of the current collector and the long life-time of the batteries. Since the obtained Li concentrations in the current collectors most likely would be very

low, the binary phase diagrams are unfortunately expected to be of limited use in these cases. Since lithium ions are unlikely to diffuse into the current collector (at least in the absence of a counter ion), the Li diffusion effect should, however, only be seen when using metallic current collectors in conjunction with Li-metal electrodes or Li-alloy-forming negative electrode materials such as Si, Sn, and Al.

Rupp et al.^[122] studied the solubility of Li in Cu employing ToF-SIMS. As shown in Figure 8a–c, lattice and grain-boundary Li diffusion were analyzed by employing single-crystal and polycrystalline Cu samples. Significant Li uptake was observed for polycrystalline Cu and the results also showed that the Li

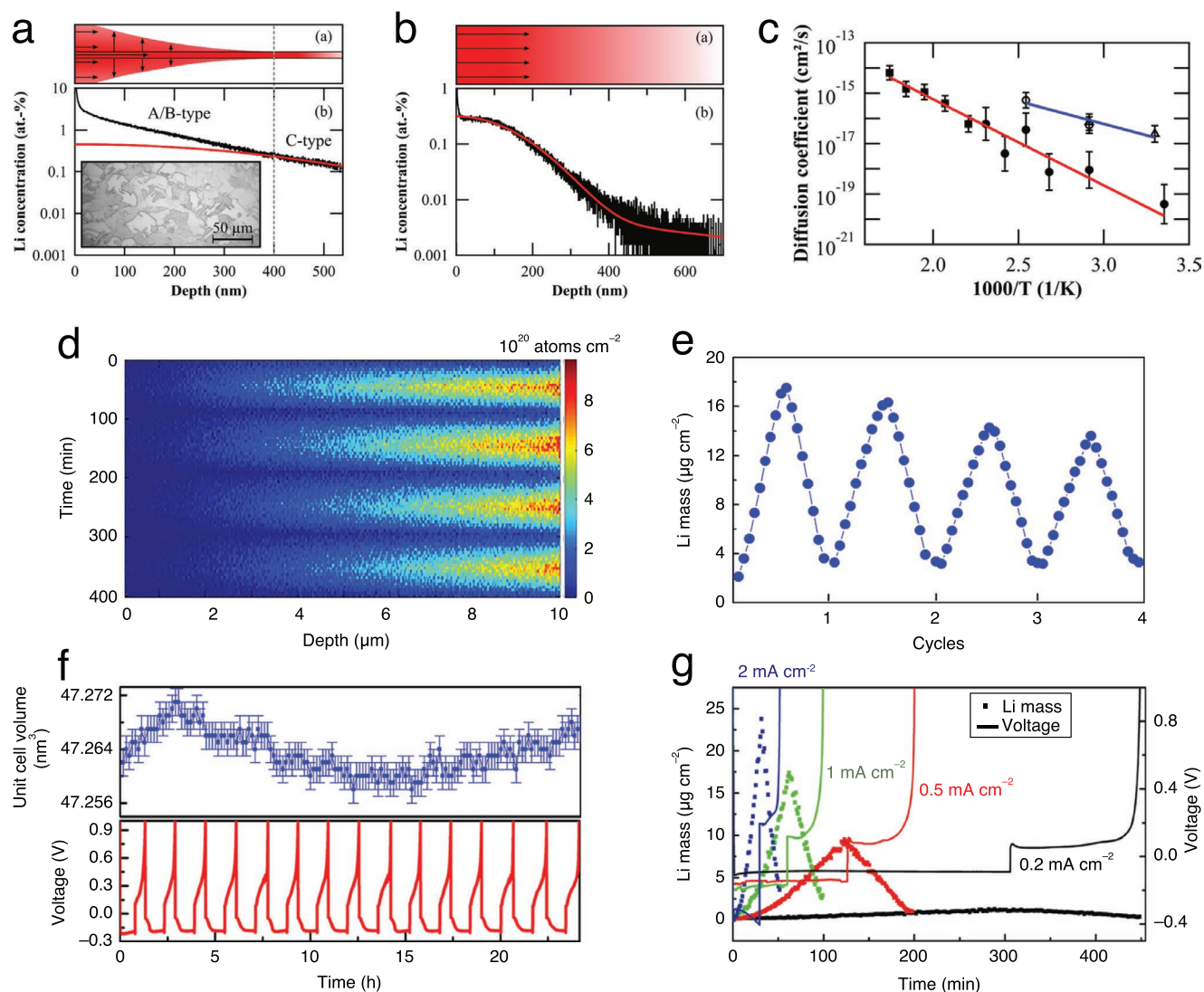


Figure 8. a) Schematic illustration of lithium diffusion into copper along a grain boundary as well as a ToF-SIMS Li concentration depth profile obtained for polycrystalline Cu exposed to metallic lithium at 120 °C for 11 days. b) Schematic representation of lithium diffusion into a copper single crystal as well as a ToF-SIMS Li concentration depth profile obtained for a single crystal Cu exposed to metallic lithium at 120 °C for 28 days. c) Arrhenius plot for Li diffusion coefficients valid for lattice diffusion in Cu single crystals (closed symbols, red fit) and grain boundary diffusion in polycrystalline Cu (open symbols, blue fit) obtained based on ToF-SIMS diffusion measurements. Reproduced with permission.^[122] Copyright 2019, American Chemical Society. d) Lithium distribution profiles within the 10 μm thick Cu current collector region during four consecutive Li deposition and oxidation cycles, as well as e) the variation in the total amounts of Li in the Cu current collector during these cycles. f) Total amount of Li found in the Cu current collector during the first deposition/oxidation cycle (as well as the corresponding cycling curves) for different current densities. g) The Cu unit cell volume as a function of time as well as the corresponding cycling curves for 15 cycles at 1.0 mA cm⁻². Reproduced with permission.^[57] Copyright 2018, Springer Nature.

diffusion rate depended on the microstructure, as smaller grains with more grain boundaries yielded larger Li diffusion rates. The latter could lead to more severe Li-trapping since the Li then can be trapped deeper within the Cu current collector. The use of large grain sized Cu was consequently suggested to limit the potential trapping of Li in these current collectors. Another alternative would be to use a conductive polycrystalline boron-doped diamond thin film as a barrier layer to limit the Li uptake by the current collectors.^[28]

Lv et al.^[57] employed operando NDP to study the Li distribution inside Cu current collectors during the deposition and oxidation of Li. During the first four cycles (Figure 8d), the concentration of Li in the Cu was found to increase and decrease while the penetration depth and the amount of Li in the current collector both increased for each cycle, indicating that the Li oxidation was incomplete. A closer look in fact revealed that while $18 \mu\text{g cm}^{-2}$ Li was found in the Cu after the first Li deposition step, only $14 \mu\text{g cm}^{-2}$ could be extracted during the following Li oxidation step (Figure 8e). This consequently indicates that $4 \mu\text{g cm}^{-2}$ of Li (i.e., about 20% of the included amount of Li) was trapped in the Cu current collector after the first cycle. On the subsequent cycles, this effect resulted in a gradual increase in the Li concentration in the Cu, and hence progressive Li-trapping (Figure 8e). The latter can explain the decrease in the maximum amount of deposited Li seen when increasing the cycle number. As shown in Figure 8f, the amount and distribution of the trapped Li depended on the current density used during cycling. A higher cycling rate (i.e., current density) hence resulted in a smaller penetration depth and a narrower Li distribution indicating that the Li uptake was diffusion controlled. Note also that the amount of Li trapped in the Cu was higher when using a higher current density. Since the uptake of Li did not affect the Cu unit cell volume determined by operando XRD (see Figure 8g), it was proposed that the Li was taken up and transported mainly within the grain boundary regions.

In an attempt to manufacture a 3D Li-metal electrode, Rehnlund et al.^[58] electrodeposited a 25 nm thin layer of Li on a copper nanorod current collector and subsequently cycled this electrode versus an analogous 3D $\text{Cu}_2\text{O}/\text{Cu}$ nanorod electrode. Despite the fact that the expected capacity of the Li/Cu electrode was four times larger than that of the $\text{Cu}_2\text{O}/\text{Cu}$ electrode, the electrochemical results clearly showed that the Li/Cu electrode became capacity limiting already after the first cycle. This phenomenon was found to stem from Li diffusing into the Cu nanorods, that is, diffusion-controlled Li-trapping. Based on this finding it is immediately clear that Li diffusion in the current collector can become a problem when developing so called “anode-free” Li-metal batteries in which Li metal thin films are deposited directly on planar and porous Cu current collectors.^[123,124] Needless to say, the problem should be particularly pronounced when using very thin Li layers as the diffusion time should depend on the square of the diffusion length.

4. Methodologies Suitable for Studies of Diffusion-Controlled Li-Trapping

As seen in the characterization of Li-trapping in LIB battery components (i.e., Section 2) many indications of diffusion-controlled

Li-trapping can be found in the literature although few reports show straightforward evidence of the process. While this may be explained by a general unawareness of the presence of a diffusion-controlled Li-trapping phenomenon, it also reflects the difficulties associated with this type of studies as the effect generally is small during the initial cycles. Selective analytical tools and techniques are consequently required to effectively study the Li-trapping effect.

Early indications of diffusion-controlled Li-trapping can often be found by comparing the electrochemical performance during galvanostatic cycling with results obtained with techniques such as CV and electrochemical impedance spectroscopy. Li-trapping in negative electrode materials can then be detected via shifts in the lithiation (but not the delithiation) potential^[20,29,36,46] toward more negative values as this indicates an increase in the Li concentration in the electrode. Cycling protocols with different lithiation and delithiation rates can also be used as an increase in the duration of the delithiation step should decrease the influence of the diffusion-controlled trapping effect.^[20] This can, for example, be done by analyzing how the cumulative capacity losses during the cycling are affected by intermittent periods of long delithiation steps using, for example, CCCV cycling protocols.^[20,28,46] Monitoring the individual electrochemical performance of the positive and negative electrodes can likewise yield evidence of lithium losses during full-cell operation. To this end, cycled electrodes reassembled with a fresh lithium metal anode can display significant recovered capacities.^[65] When analyzing used negative electrodes in newly assembled half-cells, it is important to first delithiate the electrode. If the capacity loss can be retrieved (e.g., using a long delithiation step), the capacity loss was more likely caused by diffusion-controlled Li-trapping than SEI formation. An electrochemical protocol designed to distinguish between different types of capacity losses was recently developed and used to study recoverable lithium losses in full-cell batteries during operation.^[20,28] The presence of residual Li in delithiated electrodes can also be demonstrated via post-mortem analyses using, for example, ICP-AES,^[20] STEM-EELS,^[29] and XRD.^[125] Comparisons of the amount of Li trapped in a (delithiated) negative electrode with the cumulative capacity loss can be highly informative as the capacity corresponding to the trapped Li readily can be calculated using Faraday's law.

To further validate the presence of diffusion-controlled Li-trapping, the battery components can be investigated using a wide range of spectroscopic techniques including NMR, ICP-AES, ToF-SIMS, and XPS. Changes in the lithium content in the current collectors can be revealed with ICP-AES. Such measurements indicated that diffusion-controlled Li-trapping is possible in most metallic current collectors, with or without any intermetallic phases.^[28] XPS measurement of cycled thin-film metal oxide electrodes have also demonstrated the presence of a residual lithium-rich region on fully delithiated electrode surfaces.^[43] The residual lithium can then diffuse deeper into the material where it becomes increasingly less accessible.^[94,126]

Although the techniques mentioned above can confirm the existence of lithium trapped in electrode materials and current collectors, the information regarding the spatial distribution of the residual Li inside the battery components is typically limited. To better understand the diffusion-controlled lithium

trapping problem, powerful tools to detect and quantify the trapped Li are sorely needed. ToF-SIMS is due to its high sensitivity and in-depth resolution (≈ 1 nm), a powerful technique in this respect. Chemical maps or spectra of specific regions can then be created, hence making it possible to distinguish between SEI related components and species present within the bulk of electrode materials. ToF-SIMS has, for example, been used to obtain Li depth-profiles in V_2O_5 ,^[41,116] Si,^[95] WO_3 ,^[112] and Cu.^[122]

Neutron reflectivity (NR) is another technique capable of giving spatial distribution information as it studies small changes of the scattering length density as a function of depth. The strong scattering contrast between Li and most other electrode material elements can yield precise depth profiles for Li as a function of time. This can be used to monitor the uptake of Li in Si electrodes with different crystallographic orientations.^[88,127] In situ or in operando applications of these techniques are expected to give important new insights regarding the Li-trapping phenomenon.

Recent advances regarding the use of transmission electron microscopy (TEM) has led to the creation of nanobatteries which allow in situ investigations with near-atomic resolution.^[81,82,99] With this technology, the structural and chemical evolution of individual nanosized electrode materials can be studied in both liquid^[81,128] and solid state nanobatteries.^[82,99] The technology was, for example, used to show that nanoparticles have a critical size (i.e., ≈ 150 nm) below which their fracture is prevented during extreme lithiation.^[71,75] In situ tracking of the Li-ion dynamics in positive electrodes have also revealed that nanomaterials challenge the classical definition of Li-ion intercalation.^[81,82] In this regard, EELS offers an unchallenged Li tracking capability that when used in situ studies can provide Li chemical mapping (with nanometer resolution) in all battery components. Nomura et al.^[82] overcame the problem with the very low EELS sampling rates by developing an image treatment algorithm that rapidly could process the collected low resolution spectra to reveal the Li dynamics during the first cycle. New insights are hence expected to result from in situ chemical monitoring of the Li distribution during cycling providing data analogous to the post-mortem results obtained with STEM-EELS.^[29,82]

In situ and in operando NDP has been employed to observe the evolution of lithium deposits on Cu current collectors,^[57] as well as to monitor the lithiation/delithiation behavior of Sn^[96,129] and Al^[32] anodes giving insight in the lithium spatial distribution and elucidating the lithium trapping evolution. NDP studies of lithium are based on the stoichiometric nuclear reaction between the isotope ^6Li atoms and neutrons, resulting in two charged atoms: ^4He (2044 keV) and ^3H (2727 keV).^[96,130] Because each measured ^4He and ^3H particle represents one Li in the system of interest, NDP can measure the isotopic Li density with great accuracy as a function of the depth.^[57] Hence, NDP can provide exceptional sensitivity in the visualization and quantification of lithium transport in battery material.

Synchrotron transmission X-ray microscopy for nanoscale imaging of electrochemical reactions within a working battery is becoming increasingly more powerful with respect to battery studies. This technique can provide insights into the interfacial processes and probe Li-driven local structure changes in active materials with high resolution.^[130–132]

Elastic recoil detection analysis (ERDA) is an ion beam-based analytical technique with excellent high mass resolution. The main advantage of the technique is its precise probing of light elements such as Li due to a well-defined inelastic energy loss of both recoil and scattered primary ions. The combination of both events has been combined in coincidence ERDA to study the Li distribution in a thin-film full-cell Li-ion battery during operation.^[133]

When analyzing Li-trapping events in battery components, care must clearly be taken to determine the chemical state (i.e., Li^+ ions or Li atoms) of the studied lithium. While Li atoms are stored in negative alloy forming electrodes (e.g., Si), Li ions are required in positive intercalation-based electrodes (e.g., LFP). Care should then be taken to specify if the Li diffusion in the battery components involves Li ions or Li atoms and to design the experiments accordingly.

As previously mentioned, studies of diffusion-controlled Li-trapping are best performed with half-cells in which a Li electrode is employed as a combined counter and reference electrode with a capacity well exceeding that of the electrode to be studied. In this case, the Li metal electrode will be able to compensate for any irreversible capacity losses, for example, due to SEI formation so that the capacity of the half-cell always is limited by the capacity of the studied electrode. When studying a negative electrode material there should consequently not be any capacity losses due to SEI formation as long as the capacity of the Li metal electrode remains sufficiently high. In a full-cell (or half-cell) where the counter electrode is capacity limiting, it is clearly more difficult to study the Li-trapping in a negative electrode material as this is not capacity limiting and as the capacities of the working and counter electrodes typically are of the same order of magnitude. It can then be difficult to know which electrode limits the capacity of the cell. In a full-cell where the positive electrode is capacity limiting, both Li-trapping and SEI formation at the negative electrode will drain the capacity of the positive electrode, resulting in a decreased cell capacity.

To identify the capacity limiting effects, full-cell studies require integrated analytical tools that continuously can measure the Li amounts in both electrodes. In- and ex-situ XRD has been employed to study the Li^+ distribution inside $\text{LiNi}_{(1/3)}\text{Mn}_{(1/3)}\text{Co}_{(1/3)}\text{O}_2/\text{graphite}$ full-cells after extended cycling. Xu et al.^[125] observed a gradual decrease in Li inventory on the positive electrode while the negative electrode showed no graphitic peaks in its delithiated (i.e., oxidized) state. Instead, LiC_6 and LiC_{12} phases were detected indicating that accumulation of Li^+ had occurred in the graphite electrode after 100 cycles. The observed capacity loss may then have originated either from irreversible electrolyte reactions (e.g., continuous SEI formation) or diffusion-controlled Li-trapping losses. Continuous SEI formation should, however, cause both the positive and negative electrodes to gradually become more oxidized (i.e., delithiated) during the cycling. This stems from the fact that the irreversible SEI reactions during the charging of the cell would consume charge from the positive electrode and hence effectively decrease the degree of lithiation of the negative electrode. Diffusion-controlled Li-trapping, mainly in the negative electrode, should also consume part of the charge from the positive electrode during the charging step meaning

that the positive electrode would not be fully relithiated during the subsequent discharge. This process would, however, render the positive electrode progressively less lithiated (i.e., oxidized), while the negative electrode would become increasingly more lithiated due to the trapped Li. The obtained XRD results therefore support the hypothesis that the performance of the cell was affected by diffusion-controlled Li-trapping in the graphite electrode. Efforts to retrieve trapped Li from either electrode could be used to study this effect in more detail.

5. Identification and Circumvention of Diffusion-Controlled Lithium Trapping

The influence of the diffusion-controlled Li-trapping effect is generally difficult to detect during the initial cycles as less than 1% of the deposited or inserted Li typically becomes trapped within the electrode material per cycle. Incremental changes in the performance of electrodes or cells can, however, be followed by, for example, monitoring the cell impedance during the cycling. During extended cycling, an increased impedance, mainly affecting the lithiation step, gives rise to more and more negative electrode potentials, as has been shown for Si,^[20,22,29] TiO₂,^[36] and graphite^[47] anodes. An analogous effect has also been seen for NCM^[20,40] and LCO positive electrodes.^[46] As the lithiation and delithiation potentials are determined by the surface concentration of the reduced/oxidized forms of the relevant redox couples, the presence of potential plateaus in the cycling curves indicate steady state reaction conditions. The surface concentrations (in a negative electrode) are determined by the time domain of the lithiation step at the electrode/electrolyte interface (i.e., the applied current density) and the Li diffusion rate from the electrode surface toward the bulk of the material. Sloping potential regions thus indicate that the rates of the Li insertion and inward diffusion differ yielding an accumulation of Li at the surface which shifts the lithiation potential negatively.

One straightforward way of identifying losses due to diffusion-controlled Li-trapping in negative electrodes is to plot the capacity as a function of the square root of the (cycling) time or as a function of the duration of an open circuit pause introduced between the lithiation and delithiation steps.^[20,28,58] If a linear relationship is seen, the capacity is very likely to be controlled by a diffusion-controlled process. This in turn indicates that the observed capacity is controlled by a Li-trapping effect.

The influence of the diffusion-controlled Li-trapping clearly depends on the cycling protocol used. To decrease the Li-trapping effect for negative electrodes the efficiency of the delithiation step should be increased as much as possible. This is best done with potential controlled (rather than controlled current-based) delithiation steps. If possible, the lithiation should be done using a significantly higher rate than the delithiation step as this would generate a rather thin concentration profile in the electrode material. The drawback with this approach is of course that it would be difficult to utilize the full capacity of the electrode material. Significant differences regarding the diffusion-controlled Li-trapping effects can likewise be found when comparing full capacity cycling with partial capacity cycling, for example, using potential versus Coulombic limitation. It

was recently found that Si-C composite negative electrodes can exhibit extended stable capacity cycling when applying Coulombic limited cycling (i.e., 500 mAh g⁻¹).^[134] Coulombic limited cycling has likewise yielded positive effects on the cycling stability of alloy forming anodes such as Si.^[135–137] It was, however, clearly demonstrated that the capacity-limited protocol merely prolongs the lifetime without solving the underlying issue.^[20] While the strategy can offer temporary improved cycling stability it is important to note that it only works in combination with a high-capacity counter electrode (e.g., Li metal) in a half-cell. This principle was cleverly shown for Si-LFP full-cells using LFP electrodes with varying capacities.^[138]

In the development of more durable full-cell batteries, containing capacity-balanced electrodes, it is important to minimize the capacity losses due to diffusion-controlled Li-trapping. The strategies currently used to limit or reverse the effects of the Li-trapping are mainly focused on manipulating the Li solid state diffusion. Intermittent chronoamperometric delithiation steps can, for example, be used to extract trapped Li from Si composite electrodes.^[20] This approach was also found to effectively lower the cell impedance during the subsequent lithiation step. This is promising as it could constitute the basis of future rejuvenation strategies of cycled electrodes, similar to the procedures that have been proposed to restore degraded electrochromic devices.^[56,112]

Since the Li-trapping effect discussed in this review is a diffusion-controlled process, its influence depends on factors such as the diffusion length, diffusion coefficient, and time. As the first two normally are assumed to remain constant in battery cycling experiments, the time domain of the cycling is the only parameter that can be readily modified when trying to decrease the influence of the diffusion-controlled Li-trapping. To eliminate this effect, the time domain for lithiation of the negative electrode should be chosen so that a complete lithiation is obtained, thereby resulting in a homogeneous Li concentration in the entire electrode. While this can be realized for materials with diffusion lengths of the order of some nm,^[36] it is unfortunately very difficult to obtain with conventional electrodes. The ideal electrode could be a porous structure in which all the active material should be present in the form of entities with dimensions (i.e., Li diffusion lengths) smaller than about 100 nm since the diffusion time depends on the square of the diffusion length. Although the diffusion in the electrolyte is order of magnitudes faster than the solid-state diffusion it is still very important that all the active material can be readily accessed by the electrolyte. If this is not the case the Li-concentration in the active material at the electrode surface will become higher than that in the material close to the current collector. Another complication is that the diffusion coefficient generally decreases as the lithiation degree of the electrode material becomes high enough.^[20,84] The use of a higher temperature during the delithiation step is unfortunately not likely to result in a decreased diffusion-controlled Li-trapping effect since this will increase the diffusion rate in the electrode material both toward the electrode surface and toward the current collector.

As indicated above, the influence of the diffusion-controlled Li-trapping effect can be decreased by decreasing the dimensions (e.g., particle size) of the electrode material. This, however,

also has another advantage since materials with dimensions smaller than 150 nm are known to withstand large volume expansions without breaking.^[71,75,99] By decreasing the dimensions to 10 nm, it has been found that it is possible to obtain close to theoretical capacities which remain stable during prolonged cycling.^[31] Since the use of nanoparticles affect all known capacity loss mechanisms (i.e., volume expansion, SEI/CEI formation and Li-trapping), it is sometimes difficult to know what causes the observed capacity losses. A reduced particle size increases the overall surface area which should give larger irreversible capacity losses due to continuous SEI/CEI formation.^[71,99] Capacity losses due to SEI and CEI formation, should, however, not be seen when cycling electrodes versus Li-metal electrodes in half-cells. From this point of view the small capacity losses seen for, for example, 10 nm-sized electrode materials are very promising as these results indicate that the influence of the diffusion-controlled Li-trapping effect can be made small. One significant problem with downsizing of the electrode dimensions is that it often is difficult to obtain a sufficiently high mass loading (i.e., capacity) of the active electrode materials without jeopardizing the advantageous nano effects. When the nanoparticles are packed into a dense film the diffusion length often becomes defined by the film thickness rather than the particle thickness.

The degree of diffusion-controlled Li-trapping can in principle also be reduced by increasing the Li diffusion coefficient in the electrode material. This is, however, clearly a very difficult task as the diffusion coefficients would need to be increased by orders of magnitude. Zhu et al.,^[139] nevertheless, tried to address the Li-trapping in Si negative electrodes by increasing the Li diffusion coefficient in the Si via isovalent isomorphism. The latter strategy is unfortunately very unlikely to solve the diffusion-controlled Li-trapping problem since an increased Li diffusion coefficient should affect both the lithiation and delithiation steps in the two-way diffusion equally. So, if the increase in the diffusion coefficient does not result in a complete lithiation and delithiation of the electrode material, the diffusion-controlled Li-trapping effect should remain essentially unaffected.

As indicated above, the most promising approach is to carefully design the cycling conditions so that the time domain of the experiment is compatible with the diffusion distances within the electrode material. This would reduce the influence of the two-way diffusion effect, which should result in electrodes with increased life-times.

6. Conclusions and Outlook

Based on the results discussed in this report, it is reasonable to conclude that capacity losses due to diffusion-controlled Li-trapping can be seen for both negative and positive electrode materials. As it is clear that Li-trapping likewise can take place in current collectors, the effect should also be present in anode-free lithium metal electrodes. This means that diffusion-controlled Li-trapping effects always should be considered (in addition to, e.g., SEI effects) when trying to improve the life-times of individual electrodes and full-cell batteries. Since the diffusion-controlled Li-trapping effect is due to the presence

of concentration gradients in the electrode materials it is clear that the lithiation and delithiation in these cases do not result in homogeneous concentrations of Li in the electrode materials. This implies that the solid-state diffusion rates are too low to ensure that the lithiation and delithiation steps can be conducted under equilibrium conditions. Since diffusion-controlled Li-trapping can be seen for both Li insertion and Li alloy forming electrodes, either lithium ions or lithium atoms can therefore be involved in the trapping process. The corresponding trapping effect should, incidentally, also be expected to be present in other alkali metal-based cells. The trapping stems from a mismatch between the lithiation and delithiation capacities caused by a two-way diffusion phenomenon resulting from the Li concentration profiles generated in the materials during the cycling. For a negative alloy forming electrode material, such as Si, the delithiation step becomes incomplete as a small fraction (e.g., <1%) of the deposited lithium can diffuse so far into the electrode (i.e., toward the current collector) to become inaccessible in the time domain of the subsequent delithiation step. When the amount of trapped Li in the negative electrode increases, the Li diffusion rate in the material decreases and it becomes increasingly difficult to lithiate the electrode. The capacity of the negative electrode consequently decreases while an increase in the lithiation overpotential is seen, especially during the final stages of the cycling. For a positive electrode material, the concentration gradients present in the electrode material instead result in problems to fully lithiate the positive electrode. While diffusion-controlled Li-trapping effects clearly also should give rise to capacity losses in full-cell experiments, the interpretation of such experiments is complicated by the presence of, for example, SEI and CEI effects.

The diffusion-controlled Li-trapping effect is best studied with half-cells containing the electrode of interest and a Li-metal electrode, as the capacity of such a cell should only depend on the capacity of the electrode of interest. This means that any observed decrease in the capacity cannot be explained by, for example, SEI effects. Studies of the diffusion-controlled Li-trapping effect are facilitated by the use of highly sensitive *in situ/in operando* techniques and long-term cycling experiments. Reports show that techniques such as NMR, ICP-OES, XPS, XRD, NR, ToF-SIMS, STEM-EELS, and NPD can be used to investigate the presence of capacity losses due to Li-trapping. Techniques that offer high spatial Li resolution will consequently be particularly well-suited for use in trapping studies.

There are still relatively only a few reports dealing with strategies aimed at decreasing the capacity losses due to diffusion-controlled Li-trapping. Conventional approaches designed to improve the battery capacity via modifications of the SEI layer (involving, e.g., artificial SEI layers or electrolyte engineering) are unfortunately not expected to be successful when it comes to decreasing the capacity losses due to diffusion-controlled Li-trapping. More promising approaches for negative electrode materials include the use of prolonged delithiation steps at constant potentials which increase the efficiency of the delithiation step by extending the time domain of the latter step. To eliminate capacity losses due to diffusion-controlled Li-trapping for a negative electrode material, the material must be able to undergo complete lithiation and delithiation on the time domain of the cycling. While this should be possible to achieve

for electrode materials with diffusion lengths of less than 100 nm (e.g., freestanding TiO₂ nanotube electrodes or Si nanoparticles immobilized on a conducting surface), it is unlikely to be successful for conventional electrode materials. In conventional electrode materials Li-concentration gradients will generally be present in the electrode (e.g., in the individual particles or within the electrode as a whole) which will give rise to diffusion-controlled Li-trapping effects. While thicker electrodes with higher capacities can be used to increase the capacity of a battery this also increases the risk of increasing the capacity losses due to diffusion-controlled Li-trapping since the diffusion time is proportional to the square of the diffusion length. There is hence a need for the development of new (sufficiently porous) electrode materials in which all parts of the material are equally accessible by the electrolyte and where the diffusion length in the active material is sufficiently short to allow a complete lithiation and delithiation on the time-scale of the charge and discharge steps. An alternative approach involves the development of procedures that can be used for rejuvenation of cycled electrodes and batteries. Since the capacity losses due to diffusion-controlled Li-trapping merely are caused by an inability to balance the efficiencies of the lithiation and delithiation steps rather than an irreversible degradation of the electrodes, the possibility to restore used electrodes and batteries by reversing the diffusion-controlled Li-trapping effect clearly offers exciting new possibilities.

Acknowledgements

Financial support from the Swedish Research Council (VR-2019-04276 and VR-2017-06320), StandUp and The Ångström Advanced Battery Center is gratefully acknowledged. The Outstanding Youth Scientist Foundation of Hunan Province, China (Grant No. 2021JJ10017) is acknowledged.

Conflict of Interest

The authors declare no conflict of interest.

Keywords

aging, capacity decrease, concentration gradients, diffusion, lithium redistribution, lithium trapping, lithium-based batteries

Received: November 2, 2021

Revised: February 15, 2022

Published online: March 15, 2022

[1] M. Winter, B. Barnett, K. Xu, *Chem. Rev.* **2018**, *118*, 11433.

[2] M. Winter, R. J. Brodd, *Chem. Rev.* **2004**, *104*, 4245.

[3] M. R. Palacín, A. de Guibert, *Science* **2016**, *351*, 6273.

[4] M. R. Palacín, *Chem. Soc. Rev.* **2018**, *47*, 4924.

[5] M. S. Whittingham, *Chem. Rev.* **2004**, *104*, 4271.

[6] Z. Zhu, A. Kushima, Z. Yin, L. Qi, K. Amine, J. Lu, J. Li, *Nat. Energy* **2016**, *1*, 16111.

[7] K. Luo, M. R. Roberts, R. Hao, N. Guerrini, D. M. Pickup, Y.-S. Liu, K. Edström, J. Guo, A. V. Chadwick, L. C. Duda, P. G. Bruce, *Nat. Chem.* **2016**, *8*, 684.

[8] M. Ebner, F. Marone, M. Stampanoni, V. Wood, *Science* **2013**, *342*, 716.

[9] M. N. Obrovac, V. L. Chevrier, *Chem. Rev.* **2014**, *114*, 11444.

[10] M. Park, X. Zhang, M. Chung, G. B. Less, A. M. Sastry, *J. Power Sources* **2010**, *195*, 7904.

[11] Z. Lu, N. Liu, H.-W. Lee, J. Zhao, W. Li, Y. Li, Y. Cui, *ACS Nano* **2015**, *9*, 2540.

[12] B. L.-H. Hu, F.-Y. Wu, C.-T. Lin, A. N. Khlobystov, L.-J. Li, *Nat. Commun.* **2013**, *4*, 1687.

[13] Y. Li, K. Yan, H.-W. Lee, Z. Lu, N. Liu, Y. Cui, *Nat. Energy* **2016**, *1*, 15029.

[14] U. Kasavajjula, C. Wang, A. J. Appleby, *J. Power Sources* **2007**, *163*, 1003.

[15] J. Graetz, C. Ahn, R. Yazami, B. Fultz, *Electrochem. Solid-State Lett.* **2003**, *6*, A194.

[16] H. Wang, S. Liu, Y. Ren, W. Wang, A. Tang, *Energy Environ. Sci.* **2012**, *5*, 6173.

[17] A. M. Haregewoin, A. S. Wotango, B. J. Hwang, *Energy Environ. Sci.* **2016**, *9*, 1955.

[18] H. Dai, K. Xi, X. Liu, C. Lai, S. Zhang, *J. Am. Chem. Soc.* **2018**, *140*, 17515.

[19] C. Xu, F. Lindgren, B. Philippe, M. Gorgoi, F. Björefors, K. Edström, T. Gustafsson, *Chem. Mater.* **2015**, *27*, 2591.

[20] F. Lindgren, D. Rehnlund, R. Pan, J. Pettersson, R. Younesi, C. Xu, T. Gustafsson, K. Edström, L. Nyholm, *Adv. Energy Mater.* **2019**, *9*, 1901608.

[21] A. L. Michan, G. Divitini, A. J. Pell, M. Leskes, C. Ducati, C. P. Grey, *J. Am. Chem. Soc.* **2016**, *138*, 7918.

[22] T. Yoon, C. C. Nguyen, D. M. Seo, B. L. Lucht, *J. Electrochem. Soc.* **2015**, *162*, A2325.

[23] R. Jung, M. Metzger, D. Haering, S. Solchenbach, C. Marino, N. Tsiouvaras, C. Stinner, H. A. Gasteiger, *J. Electrochem. Soc.* **2016**, *163*, A1705.

[24] J. Vetter, P. Novák, M. R. Wagner, C. Veit, K. C. Möller, J. O. Besenhard, M. Winter, M. Wohlfahrt-Mehrens, C. Vogler, A. Hammouche, *J. Power Sources* **2005**, *147*, 269.

[25] G. Ji, Y. Ma, J. Y. Lee, *J. Mater. Chem.* **2011**, *21*, 9819.

[26] Z. Wang, C. Xu, P. Tammela, J. Huo, M. Strømme, K. Edstrom, T. Gustafsson, L. Nyholm, *J. Mater. Chem. A* **2015**, *3*, 14109.

[27] Y. Eker, K. Kierzek, E. Raymundo-Piñero, J. Machnikowski, F. Béguin, *Electrochim. Acta* **2010**, *55*, 729.

[28] D. Rehnlund, F. Lindgren, S. Böhme, T. Nordh, Y. Zou, J. Pettersson, U. Bexell, M. Boman, K. Edström, L. Nyholm, *Energy Environ. Sci.* **2017**, *10*, 1350.

[29] P. Kumar, C. L. Berhaut, D. Zapata Dominguez, E. De Vito, S. Tardif, S. Pouget, S. Lyonnard, P. H. Jouneau, *Small* **2020**, *16*, 1906812.

[30] F. Holtstiege, A. Wilken, M. Winter, T. Placke, *Phys. Chem. Chem. Phys.* **2017**, *19*, 25905.

[31] H. Kim, M. Seo, M. H. Park, J. Cho, *Angew. Chem., Int. Ed.* **2010**, *49*, 2146.

[32] D. X. Liu, A. C. Co, *J. Am. Chem. Soc.* **2016**, *138*, 231.

[33] B. Qin, T. Diemant, H. Zhang, A. Hoefling, R. J. Behm, J. Tübke, A. Varzi, S. Passerini, *ChemSusChem* **2019**, *12*, 2609.

[34] N. S. Hudak, D. L. Huber, *J. Electrochem. Soc.* **2012**, *159*, A688.

[35] G. Oltean, C.-W. Tai, K. Edström, L. Nyholm, *J. Power Sources* **2014**, *269*, 266.

[36] W. Wei, C. Ihrfors, F. Björefors, L. Nyholm, *ACS Appl. Energy Mater.* **2020**, *3*, 4638.

[37] A. S. Andersson, B. Kalska, L. Häggström, J. O. Thomas, *Solid State Ionics* **2000**, *130*, 41.

[38] A. Andersson, J. O. Thomas, *J. Power Sources* **2001**, *97*, 498.

[39] R. Pan, R. Sun, Z. Wang, J. Lindh, K. Edström, M. Strømme, L. Nyholm, *Energy Storage Mater.* **2019**, *21*, 464.

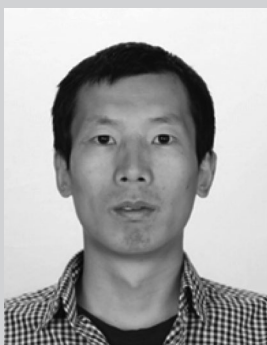
[40] J. Kasnatscheew, M. Evertz, B. Streipert, R. Wagner, S. Nowak, I. Cekic Laskovic, M. Winter, *J. Phys. Chem. C* **2017**, *121*, 1521.

- [41] D. Alamarguy, J. E. Castle, M. Liberatore, F. Decker, *Surf. Interface Anal.* **2006**, *38*, 847.
- [42] Y. Sakurai, S. Okada, J. Yamaki, T. Okada, *J. Power Sources* **1987**, *20*, 173.
- [43] J. Światowska-Mrowiecka, V. Maurice, S. Zanna, L. Klein, P. Marcus, *Electrochim. Acta* **2007**, *52*, 5644.
- [44] H.-K. Kim, T.-Y. Seong, Y. S. Yoon, *J. Vac. Sci. Technol., B: Microelectron. Nanometer Struct.–Process., Meas., Phenom.* **2003**, *21*, 754.
- [45] J. Światowska-Mrowiecka, S. de Diesbach, V. Maurice, S. Zanna, L. Klein, E. Briand, I. Vickridge, P. Marcus, *J. Phys. Chem. C* **2008**, *112*, 11050.
- [46] R. Pan, D. Rau, Y. Moryson, J. Sann, J. r. Janek, *ACS Appl. Energy Mater.* **2020**, *3*, 6065.
- [47] B. P. Matadi, S. Geniès, A. Delaille, C. Chabrol, E. de Vito, M. Bardet, J.-F. Martin, L. Daniel, Y. Bultel, *J. Electrochem. Soc.* **2017**, *164*, A2374.
- [48] K. P. C. Yao, J. S. Okasinski, K. Kalaga, I. A. Shkrob, D. P. Abraham, *Energy Environ. Sci.* **2019**, *12*, 656.
- [49] W. Xing, J. Dahn, *J. Electrochem. Soc.* **1997**, *144*, 1195.
- [50] Y. Matsumura, S. Wang, J. Mondori, *J. Electrochem. Soc.* **1995**, *142*, 2914.
- [51] E. Jacques, M. Hellqvist Kjell, D. Zenkert, G. Lindbergh, M. Behm, *Carbon* **2013**, *59*, 246.
- [52] K. Guerin, A. Fevrier-Bouvier, S. Flandrois, B. Simon, P. Biensan, *Electrochim. Acta* **2000**, *45*, 1607.
- [53] M. Winter, P. Novák, A. Monnier, *J. Electrochem. Soc.* **1998**, *145*, 428.
- [54] N. Takami, A. Satoh, T. Ohsaki, M. Kanda, *J. Electrochem. Soc.* **1998**, *145*, 478.
- [55] D. Dong, W. Wang, A. Rougier, A. Barnabé, G. Dong, F. Zhang, X. Diao, *J. Mater. Chem. C* **2018**, *6*, 9875.
- [56] R.-T. Wen, C. G. Granqvist, G. A. Niklasson, *Nat. Mater.* **2015**, *14*, 996.
- [57] S. Lv, T. Verhallen, A. Vasileiadis, F. Ooms, Y. Xu, Z. Li, Z. Li, M. Wagemaker, *Nat. Commun.* **2018**, *9*, 2152.
- [58] D. Rehnlund, J. Pettersson, K. Edström, L. Nyholm, *ChemistrySelect* **2018**, *3*, 2311.
- [59] E. Peled, *J. Electrochem. Soc.* **1979**, *126*, 2047.
- [60] S. E. Sloop, J. B. Kerr, K. Kinoshita, *J. Power Sources* **2003**, *119*, 330.
- [61] M. Gauthier, T. J. Carney, A. Grimaud, L. Giordano, N. Pour, H.-H. Chang, D. P. Fenning, S. F. Lux, O. Paschos, C. Bauer, *J. Phys. Chem. Lett.* **2015**, *6*, 4653.
- [62] V. Etacheri, O. Haik, Y. Goffer, G. A. Roberts, I. C. Stefan, R. Fasching, D. Aurbach, *Langmuir* **2011**, *28*, 965.
- [63] S. Dalavi, P. Guduru, B. L. Lucht, *J. Electrochem. Soc.* **2012**, *159*, A642.
- [64] B. T. Young, D. R. Heskett, C. C. Nguyen, M. Nie, J. C. Woicik, B. L. Lucht, *ACS Appl. Mater. Interfaces* **2015**, *7*, 20004.
- [65] N. Delpuech, N. Dupre, P. Moreau, J. S. Bridel, J. Gaubicher, B. Lestriez, D. Guyomard, *ChemSusChem* **2016**, *9*, 841.
- [66] Q. Ai, D. Li, J. Guo, G. Hou, Q. Sun, Q. Sun, X. Xu, W. Zhai, L. Zhang, J. Feng, P. Si, J. Lou, L. Ci, *Adv. Mater. Interfaces* **2019**, *6*, 1901187.
- [67] Y. Cao, M. Li, J. Lu, J. Liu, K. Amine, *Nat. Nanotechnol.* **2019**, *14*, 200.
- [68] J. H. Ryu, J. W. Kim, Y.-E. Sung, S. M. Oh, *Electrochem. Solid-State Lett.* **2004**, *7*, A306.
- [69] R. A. Huggins, W. D. Nix, *Ionics* **2000**, *6*, 57.
- [70] M. N. Obrovac, L. Christensen, *Electrochem. Solid-State Lett.* **2004**, *7*, A93.
- [71] X. H. Liu, L. Zhong, S. Huang, S. X. Mao, T. Zhu, J. Y. Huang, *ACS Nano* **2012**, *6*, 1522.
- [72] D. Ma, Z. Cao, A. Hu, *Nano-Micro Lett.* **2014**, *6*, 347.
- [73] N. Liu, Z. Lu, J. Zhao, M. T. McDowell, H.-W. Lee, W. Zhao, Y. Cui, *Nat. Nanotechnol.* **2014**, *9*, 187.
- [74] S. Choi, T.-w. Kwon, A. Coskun, J. W. Choi, *Science* **2017**, *357*, 279.
- [75] M. T. McDowell, I. Ryu, S. W. Lee, C. Wang, W. D. Nix, Y. Cui, *Adv. Mater.* **2012**, *24*, 6034.
- [76] J. Guo, Z. Jia, *J. Power Sources* **2021**, *486*, 229371.
- [77] S. Nowak, M. Winter, *Acc. Chem. Res.* **2018**, *51*, 265.
- [78] J. P. Pender, G. Jha, D. H. Youn, J. M. Ziegler, I. Andoni, E. J. Choi, A. Heller, B. S. Dunn, P. S. Weiss, R. M. Penner, *ACS Nano* **2020**, *14*, 1243.
- [79] C. Xu, K. Märker, J. Lee, A. Mahadevegowda, P. J. Reeves, S. J. Day, M. F. Groh, S. P. Emge, C. Ducati, B. L. Mehdi, *Nat. Mater.* **2021**, *20*, 84.
- [80] K. Märker, P. J. Reeves, C. Xu, K. J. Griffith, C. P. Grey, *Chem. Mater.* **2019**, *31*, 2545.
- [81] W. Zhang, H.-C. Yu, L. Wu, H. Liu, A. Abdellahi, B. Qiu, J. Bai, B. Orvananos, F. C. Strobridge, X. Zhou, Z. Liu, G. Ceder, Y. Zhu, K. Thornton, C. P. Grey, F. Wang, *Sci. Adv.* **2018**, *4*, eaao2608.
- [82] Y. Nomura, K. Yamamoto, M. Fujii, T. Hirayama, E. Igaki, K. Saitoh, *Nat. Commun.* **2020**, *11*, 2824.
- [83] J. Kasnatscheew, M. Evertz, B. Streipert, R. Wagner, R. Klöpsch, B. Vortmann, H. Hahn, S. Nowak, M. Amereller, A.-C. Gentschew, *Phys. Chem. Chem. Phys.* **2016**, *18*, 3956.
- [84] H. Zhou, F. Xin, B. Pei, M. S. Whittingham, *ACS Energy Lett.* **2019**, *4*, 1902.
- [85] F. Friedrich, B. Strehle, A. T. Freiberg, K. Kleiner, S. J. Day, C. Er, M. Piana, H. A. Gasteiger, *J. Electrochem. Soc.* **2019**, *166*, A3760.
- [86] J. Li, N. J. Dudney, X. Xiao, Y. T. Cheng, C. Liang, M. W. Verbrugge, *Adv. Energy Mater.* **2015**, *5*, 1401627.
- [87] J. Kim, W. Lee, J. Seok, E. Lee, W. Choi, H. Park, S. Yun, M. Kim, J. Lim, W.-S. Yoon, *J. Energy Chem.* **2022**, *66*, 226.
- [88] B.-K. Seidlhofer, B. Jerliu, M. Trapp, E. Hüger, S. Risse, R. Cubitt, H. Schmidt, R. Steitz, M. Ballauff, *ACS Nano* **2016**, *10*, 7458.
- [89] T. M. Higgins, S. H. Park, P. J. King, C. J. Zhang, N. McEvoy, N. C. Berner, D. Daly, A. Shmeliov, U. Khan, G. Duesberg, V. Nicolosi, J. N. Coleman, *ACS Nano* **2016**, *10*, 3702.
- [90] M. H. Ryu, J. Kim, I. Lee, S. Kim, Y. K. Jeong, S. Hong, J. H. Ryu, T. S. Kim, J. K. Park, H. Lee, *Adv. Mater.* **2013**, *25*, 1571.
- [91] V. Chakrapani, F. Rusli, M. A. Filler, P. A. Kohl, *J. Power Sources* **2012**, *205*, 433.
- [92] C. Chen, J. F. M. Oudenhoven, D. L. Danilov, E. Vezhlev, L. Gao, N. Li, F. M. Mulder, R.-A. Eichel, P. H. L. Notten, *Adv. Energy Mater.* **2018**, *8*, 1801430.
- [93] J. G. Lee, J. Kim, H. Park, J. B. Lee, J. H. Ryu, J. J. Kim, S. M. Oh, *J. Electrochem. Soc.* **2015**, *162*, A1579.
- [94] C. Pereira-Nabais, J. Światowska, M. Rosso, F. Ozanam, A. Seyeux, A. Gohier, P. Tran-Van, M. Cassir, P. Marcus, *ACS Appl. Mater. Interfaces* **2014**, *6*, 13023.
- [95] A. Bordes, E. De Vito, C. Haon, A. Boulineau, A. Montani, P. Marcus, *Chem. Mater.* **2016**, *28*, 1566.
- [96] D. X. Liu, J. Wang, K. Pan, J. Qiu, M. Canova, L. R. Cao, A. C. Co, *Angew. Chem., Int. Ed.* **2014**, *53*, 9498.
- [97] H. Li, L. Shi, W. Lu, X. Huang, L. Chen, *J. Electrochem. Soc.* **2001**, *148*, A915.
- [98] M. S. Leite, D. Ruzmetov, Z. Li, L. A. Bendersky, N. C. Bartelt, A. Kolmakov, A. A. Talin, *J. Mater. Chem. A* **2014**, *2*, 20552.
- [99] X. H. Liu, Y. Liu, A. Kushima, S. Zhang, T. Zhu, J. Li, J. Y. Huang, *Adv. Energy Mater.* **2012**, *2*, 722.
- [100] R. E. Franklin, *Acta Crystallogr.* **1951**, *4*, 253.
- [101] H. Kim, J. Hong, K. Y. Park, H. Kim, S. W. Kim, K. Kang, *Chem. Rev.* **2014**, *114*, 11788.
- [102] K. Guérin, M. Ménétrier, A. Février-Bouvier, S. Flandrois, B. Simon, P. Biensan, *Solid State Ionics* **2000**, *127*, 187.
- [103] N. Holzwarth, S. G. Louie, S. Rabbii, *Phys. Rev. B* **1983**, *28*, 1013.
- [104] E. Jacques, M. H. Kjell, D. Zenkert, G. Lindbergh, *Carbon* **2014**, *68*, 725.
- [105] S. Böhme, K. Edström, L. Nyholm, *J. Electroanal. Chem.* **2017**, *797*, 47.

- [106] S. Böhme, K. Edström, L. Nyholm, *Electrochim. Acta* **2015**, *179*, 482.
- [107] M. Valvo, M. Roberts, G. Oltean, B. Sun, D. Rehnlund, D. Brandell, L. Nyholm, T. Gustafsson, K. Edström, *J. Mater. Chem. A* **2013**, *1*, 9281.
- [108] D. Rehnlund, M. Valvo, C.-W. Tai, J. Ångström, M. Sahlberg, K. Edström, L. Nyholm, *Nanoscale* **2015**, *7*, 13591.
- [109] J. Bisquert, *Electrochim. Acta* **2002**, *47*, 2435.
- [110] M. Strømme Mattsson, *Solid State Ionics* **2000**, *131*, 261.
- [111] R.-T. Wen, M. A. Arvizu, M. Morales-Luna, C. G. Granqvist, G. A. Niklasson, *Chem. Mater.* **2016**, *28*, 4670.
- [112] B. Baloukas, M. A. Arvizu, R.-T. Wen, G. A. Niklasson, C. G. Granqvist, R. Vernhes, J. E. Klemberg-Sapieha, L. Martinu, *ACS Appl. Mater. Interfaces* **2017**, *9*, 16995.
- [113] C. G. Granqvist, M. A. Arvizu, İ. Bayrak Pehlivan, H. Y. Qu, R. T. Wen, G. A. Niklasson, *Electrochim. Acta* **2018**, *259*, 1170.
- [114] L.-X. Yuan, Z. Wang, W.-X. Zhang, X.-L. Hu, J.-T. Chen, Y.-H. Huang, J. B. Goodenough, *Energy Environ. Sci.* **2011**, *4*, 269.
- [115] A. S. Andersson, J. O. Thomas, B. Kalska, L. Häggström, *Electrochim. Solid-State Lett.* **2000**, *3*, 66.
- [116] J. Światowska-Mrowiecka, F. Martin, V. Maurice, S. Zanna, L. Klein, J. Castle, P. Marcus, *Electrochim. Acta* **2008**, *53*, 4257.
- [117] J. Kasnatscheew, M. Evertz, B. Streipert, R. Wagner, R. Klöpsch, B. Vortmann, H. Hahn, S. Nowak, M. Amereller, A. C. Gentschev, P. Lamp, M. Winter, *Phys. Chem. Chem. Phys.* **2016**, *18*, 3956.
- [118] C. Hong, Q. Leng, J. Zhu, S. Zheng, H. He, Y. Li, R. Liu, J. Wan, Y. Yang, *J. Mater. Chem. A* **2020**, *8*, 8540.
- [119] H. Okamoto, *J. Phase Equilib. Diffus.* **2011**, *32*, 172.
- [120] B. Predel, in Li-Ni (Lithium-Nickel). *Li-Mg-Nd-Zr*, Landolt-Börnstein - Group IV Physical Chemistry, *5H*, Springer, New York **1990**, p. 1. https://materials.springer.com/lb/docs/sm_lbs_978-3-540-68538-8_1911.
- [121] C. Bale, *Bull. Alloy Phase Diagrams* **1989**, *10*, 135.
- [122] R. Rupp, B. Caerts, A. Vantomme, J. Fransaer, A. Vlad, *J. Phys. Chem. Lett.* **2019**, *10*, 5206.
- [123] J. Qian, B. D. Adams, J. Zheng, W. Xu, W. A. Henderson, J. Wang, M. E. Bowden, S. Xu, J. Hu, J.-G. Zhang, *Adv. Funct. Mater.* **2016**, *26*, 7094.
- [124] C. P. Yang, Y. X. Yin, S. F. Zhang, N. W. Li, Y. G. Guo, *Nat. Commun.* **2015**, *6*, 8058.
- [125] C. Xu, F. Jeschull, W. R. Brant, D. Brandell, K. Edström, T. Gustafsson, *J. Electrochem. Soc.* **2018**, *165*, A40.
- [126] J.-T. Li, V. Maurice, J. Światowska-Mrowiecka, A. Seyeux, S. Zanna, L. Klein, S.-G. Sun, P. Marcus, *Electrochim. Acta* **2009**, *54*, 3700.
- [127] B. Jerliu, L. Dörrer, E. Hüger, G. Borchardt, R. Steitz, U. Geckle, V. Oberst, M. Bruns, O. Schneider, H. Schmidt, *Phys. Chem. Chem. Phys.* **2013**, *15*, 7777.
- [128] A. J. Leenheer, K. L. Jungjohann, K. R. Zavadil, C. T. Harris, *ACS Nano* **2016**, *10*, 5670.
- [129] D. X. Liu, L. R. Cao, A. C. Co, *Chem. Mater.* **2016**, *28*, 556.
- [130] C. P. Grey, J. M. Tarascon, *Nat. Mater.* **2017**, *16*, 45.
- [131] J. Wang, Y.-c. K. Chen-Wiegart, J. Wang, *Nat. Commun.* **2014**, *5*, 4570.
- [132] S. Kuppan, Y. Xu, Y. Liu, G. Chen, *Nat. Commun.* **2017**, *8*, 14309.
- [133] V. Mathayan, M. V. Moro, K. Morita, B. Tsuchiya, R. Ye, M. Baba, D. Primetzhofer, *Appl. Phys. Lett.* **2020**, *117*, 023902.
- [134] K. Yao, J. P. Zheng, Z. Liang, *ACS Appl. Mater. Interfaces* **2018**, *10*, 7155.
- [135] M. Obrovac, L. Krause, *J. Electrochem. Soc.* **2007**, *154*, A103.
- [136] H. T. Nguyen, M. R. Zamfir, L. D. Duong, Y. H. Lee, P. Bondavalli, D. Pribat, *J. Mater. Chem.* **2012**, *22*, 24618.
- [137] L. Leveau, B. Laïk, J.-P. Pereira-Ramos, A. Gohier, P. Tran-Van, C.-S. Cojocar, *Electrochim. Acta* **2015**, *157*, 218.
- [138] W. M. Dose, V. A. Maroni, M. J. Piernas-Muñoz, S. E. Trask, I. Bloom, C. S. Johnson, *J. Electrochem. Soc.* **2018**, *165*, A2389.
- [139] B. Zhu, G. Liu, G. Lv, Y. Mu, Y. Zhao, Y. Wang, X. Li, P. Yao, Y. Deng, Y. Cui, J. Zhu, *Sci. Adv.* **2019**, *5*, eaax0651.



David Rehnlund is a young investigator in electrochemical energy storage at Uppsala University, Sweden. After completing his master in chemical engineering (2011), he continued with his doctoral studies on electrochemical synthesis and characterization of nanostructured electrodes for Li-ion batteries resulting in a Ph.D. degree (2015) from Uppsala University, Sweden. During his postdoctoral research (2016–2021) he developed electrochemical strategies to control Li metal growth and nanostructured electrodes that can interface with electroactive bacteria at Uppsala University, Sweden and Karlsruhe Institute of Technology, Germany. His research interests span from alkali-metal electrodes in rechargeable batteries to microbial bioelectrochemical energy storage.



Zhaohui Wang is a professor of materials science at Hunan University, China. He received his B.E. (2007), M.E. (2009), and Ph.D. degree (2012) from Huazhong University of Science and Technology, China. He had worked at Uppsala University as researcher during 2013–2020, focusing on the research of nanostructured conducting polymer composites and paper batteries. His current research interests include the value-added utilization of cellulose-based functional materials, for example, design of cellulose-based separator, paper-based electrodes, and flexible current collectors, and the development of biomass-based high energy density energy storage devices.



Leif Nyholm, who holds a position as professor at the Department of Chemistry-Ångström Laboratory at Uppsala University, Sweden, obtained his Ph.D. in Analytical Chemistry in 1989 and worked as a postdoc at Southampton University, UK, between 1990 and 1992. His current work includes research on lithium-based batteries involving, for example, lithium trapping effects, planar deposition of lithium on lithium-metal electrodes, and electrodeposition of nanostructured electrodes, as well as paper-based electrochemical energy storage devices, functional cellulose-based separators, and corrosion resistant high entropy alloys.